Electronic Supplementary Material (ESI) for ChemComm.
This journal is © The Royal Society of Chemistry 2026

Supporting Information for

A quinazolinone-linked covalent organic framework with an intrinsic N-N bond for efficient palladium nanocatalysis

Xu-Hao Zhang,‡ Xiu-Hao Zhang,‡ Fu-Hao Liu,‡ Fei Li, Yan Geng,* and Bing-Jian Yao*

College of Chemistry, Chemical Engineering and Materials Science, Collaborative Innovation Center of Functionalized Probes for Chemical Imaging in Universities of Shandong, Key Laboratory of Molecular and Nano Probes, Ministry of Education, Shandong Normal University, Jinan 250014, P. R. China.

‡ These authors contributed equally to this work.

Email: gengyan@sdnu.edu.cn; yaobingjian1986@163.com

Content

1. Experimental section

1.1 Instruments and materials

All chemicals were purchased from commercial suppliers and used without further purification unless otherwise specified. Fourier-transform infrared (FTIR) spectra were recorded on a Bruker ALPHA spectrometer in the wavenumber range of 500-4000 cm^{-1}. High-resolution mass spectra (HRMS) were acquired using a Bruker maXis ultra-high-resolution time-of-flight mass spectrometer. Elemental analyses were performed on a PerkinElmer 2400 Series II CHNS/O analyzer. Solution-state ^{1}H and ^{13}C nuclear magnetic resonance (NMR) spectra were obtained on a Bruker Avance-400 HD spectrometer operating at 400 MHz and 100 MHz, respectively. Solid-state ^{13}C cross-polarization magic-angle spinning (CP-MAS) NMR spectra were acquired on a Varian Mercury Plus 400 spectrometer at a ^{13}C resonance frequency of 100 MHz. Powder X-ray diffraction (PXRD) patterns were collected on a Bruker D8 Advance diffractometer equipped with Cu Kα radiation (λ = 1.5406 Å), using a flat-plate sample holder and step-scanning mode. Scanning electron microscopy (SEM) images and energy-dispersive X-ray (EDX) spectroscopy data were acquired on a Zeiss Gemini SUPRA microscope. Transmission electron microscopy (TEM) images were recorded on a JEOL JEM-1400Plus instrument operated at 120 kV. Nitrogen adsorption-desorption isotherms were measured at 77 K using a Micromeritics ASAP 2020 surface area and porosity analyzer. Thermogravimetric analysis (TGA) was conducted on a METTLER TOLEDO TGA/DSC1 instrument under a flowing nitrogen atmosphere (30 mL•min^{-1}) at a heating rate of 15 °C•min^{-1}. X-ray photoelectron spectroscopy (XPS) measurements were carried out on a Physical Electronics PHI-5000 Versaprobe II system using monochromated Al Kα radiation (1486.6 eV) at 300 W. Inductively coupled plasma optical emission spectroscopy (ICP-OES) was performed on a Thermo Scientific iCAP RQ (formerly IRIS Intrepid II XSP) spectrometer; elemental quantification was validated using a Nu AttoM high-sensitivity ICP-MS where required. The monomer AABH was synthesized according to a literature procedure (see Section 1.2). The triazine-based aldehyde TFBT (1,3,5-tris-(4'-formylbiphenyl-4-yl)triazine) was purchased from Energy Chemical Co., Ltd. (Shanghai, China) and used as received.

1.2 Synthesis of 2-amino-N'-(2-aminobenzoyl) benzohydrazide (AABH)

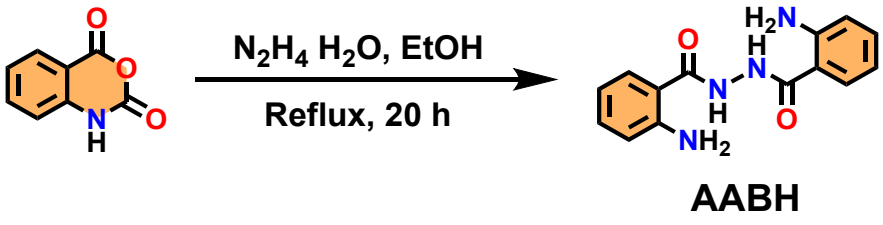

AABH

AABH was synthesized according to a literature procedure.[1] To a suspension of isatoic anhydride (5.98 g, 36.7 mmol) in anhydrous ethanol (30 mL), hydrazine hydrate (0.95 mL,19.5 mmol) was added dropwise at room temperature. The resulting mixture was refluxed with vigorous stirring for 20 h. The precipitated solid was collected by vacuum filtration, washed sequentially with ice-cold ethanol (20 mL) and diethyl ether (20 mL), and dried under vacuum to afford AABH as a brown powder (2.5 g, 9.34 mmol, 51%). ^{1}H NMR (400 MHz, DMSO-d_6, ppm): δ= 10.03 (s, 2H), 7.60 (d, 2H, J =8 Hz), 7.19 (t, 2H, J =8 Hz), 6.72 (d,

2H, *J* =12 Hz), 6.54 (t, 2H, *J* =8 Hz), 6.42 ppm (s, 4H). ^{13}C NMR (100 MHz, DMSO-d_6, ppm): δ=168.92, 150.38, 132.73, 128.65, 116.86, 115.06, 113.08. HRMS (ESI): *m/z* $[M+H]^+$ calcd for $C_{14}H_{14}N_4O_2$ 271.1190; found, 271.1183.

1.3 Synthesis of model compound

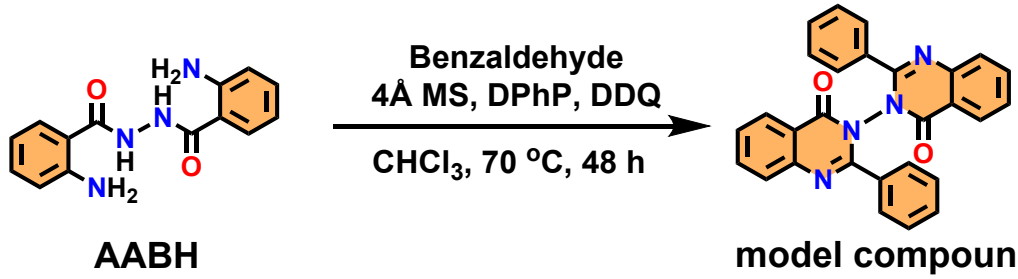

In a dried Schlenk flask equipped with a magnetic stir bar, activated 4 Å molecular sieves (200 mg) were introduced under a positive flow of argon. The flask was then charged with AABH (162 mg, 0.6 mmol), benzaldehyde (127 mg, 1.20 mmol), diphenyl phosphate (DPhP, 15 mg, 0.06 mmol), 2,3-dichloro-5,6-dicyano-1,4-benzoquinone (DDQ, 190 mg, 0.84 mmol), and chloroform (10 mL). The reaction mixture was heated to reflux in a preheated oil bath at 70 °C under a static argon atmosphere for 48 h. Upon completion, the mixture was cooled to room temperature and filtered through a celite pad to remove solids. The filtrate was concentrated under reduced pressure and the crude product was purified by flash column chromatography on silica gel (petroleum ether/ethyl acetate = 2:1) to afford the desired dual-quinazolinone as a white solid (134 mg, 95% yield). ^{1}H NMR (400 MHz, DMSO-d_6, ppm): δ= 8.39 (d, 2H, *J* =8 Hz), 8.00 (t, 2H, *J* =8 Hz), 7.74 (m, 4H, *J* =8 Hz), 7.48 (t, 2H, *J* =8 Hz), 7.36 (t, 4H, *J* =8 Hz), 7.16 ppm (d, 4H, *J* =8 Hz). ^{13}C NMR (100 MHz, DMSO-d_6, ppm): δ=159.85, 154.01, 146.61, 135.53, 132.22, 130.81, 128.31, 128.18, 127.85, 127.72, 120.83. HRMS (ESI): *m/z* $[M+H]^+$ calcd for $C_{28}H_{18}N_4O_2$ 443.1503; found, 443.1493.

1.4 Synthesis of AABH-TFBT-COF

A mixture of AABH (8.1 mg, 0.03 mmol), 1,3,5-tris-(4'-formyl-biphenyl-4-yl) triazine (TFBT, 12.4 mg, 0.02 mmol), DDQ (4.5 mg, 0.02 mmol), and DPhP (6 mg, 0.024 mmol) in mesitylene (1.0 mL) was sealed and heated at 120 °C for 5 days under air conditions. The resulting precipitate was isolated by centrifugation, washed sequentially with DMF and dichloromethane (DCM), and dried under high vacuum overnight to afford **AABH-TFBT-COF** as an off-white solid (16.5 mg, 85% yield). FTIR (KBr, cm^{-1}): 3339 (w), 1675 (s), 1610 (s), 1571 (m), 1518 (s), 1418 (w), 1365 (m), 1246 (m), 1088 (w), 1005 (w), 910 (w), 840 (w), 816 (m), 769 (m), 681 (w). ^{13}C CP-MAS solid-state NMR: δ (ppm) 190.4, 168.8, 146.9, 142.8, 140.7, 134.6, 127.3, 120.5, 115.1. Elemental analysis (%) calcd for $C_{21}H_{12}N_3O$: C, 78.27; H, 3.72; N, 13.04. Found (%): C, 77.43; H, 4.27; N, 12.60.

1.5 Synthesis of Pd@AABH-TFBT-COF

AABH-TFBT-COF (70 mg) was dispersed in a methanol solution (35 mL) containing palladium(II) acetate ($Pd(OAc)_2$, 20 mg). The suspension was stirred at 45 °C for 12 h. The solid was recovered by

centrifugation, washed repeatedly with DCM, and dried under vacuum at 60 °C for 12 h to afford **Pd(II)@AABH-TFBT-COF**. Subsequently, the obtained Pd(II)-loaded COF (70 mg) was suspended in water (30 mL) containing sodium borohydride ($NaBH_4$, 20 mg) and stirred at room temperature for 10 h. The resulting black crystalline solid was isolated by centrifugation, washed with water and ethanol, and dried under vacuum to yield **Pd@AABH-TFBT-COF** as a black crystalline powder. As determined by inductively coupled plasma (ICP), the loading amount of Pd NPs was up to 16.54 wt%

1.6 Model Suzuki-Miyaura coupling reaction catalyzed by Pd@AABH-TFBT-COF

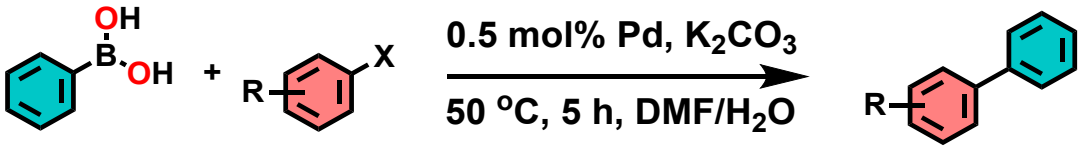

General procedure

A dried Schlenk flask was charged with **Pd@AABH-TFBT-COF** (3.3 mg, 0.5 mol% Pd nanoparticles), phenylboronic acid (1.0 mmol), bromobenzene (1.1 mmol), K_2CO_3 (1.5 mmol), and a mixed solvent system of DMF/H_2O (1.5 mL/1.5 mL). The reaction mixture was stirred at 50 °C for 5 h under an argon atmosphere, and reaction progress was monitored by thin-layer chromatography (TLC).

Leaching test

After 3 h of the Suzuki–Miyaura coupling reaction, the heterogeneous catalyst **Pd@AABH-TFBT-COF** was separated from the reaction mixture by centrifugation. The resulting catalyst-free supernatant was subjected to three vacuum–argon purge cycles to remove dissolved oxygen, then maintained at 50 °C under vigorous stirring. No further increase in biphenyl yield was detected over an additional 5 h, confirming that catalytic activity is attributable solely to the solid-supported palladium species and not to leached Pd species in solution.

Reusability assessment

Upon completion of each catalytic cycle, the **Pd@AABH-TFBT-COF** catalyst was recovered by centrifugation, washed sequentially with fresh reaction solvent (DMF/H_2O, 3×15 mL) followed by petroleum ether (3×15 mL) to remove residual organic species and salts, and dried under reduced pressure. The recovered catalyst was reused directly in subsequent runs without chemical or thermal regeneration. For the recycling experiments, a 10 mmol scale reaction (33 mg of catalyst per cycle, corresponding to 0.5 mol% Pd) was performed.

2.Characterization of model compound and monomers

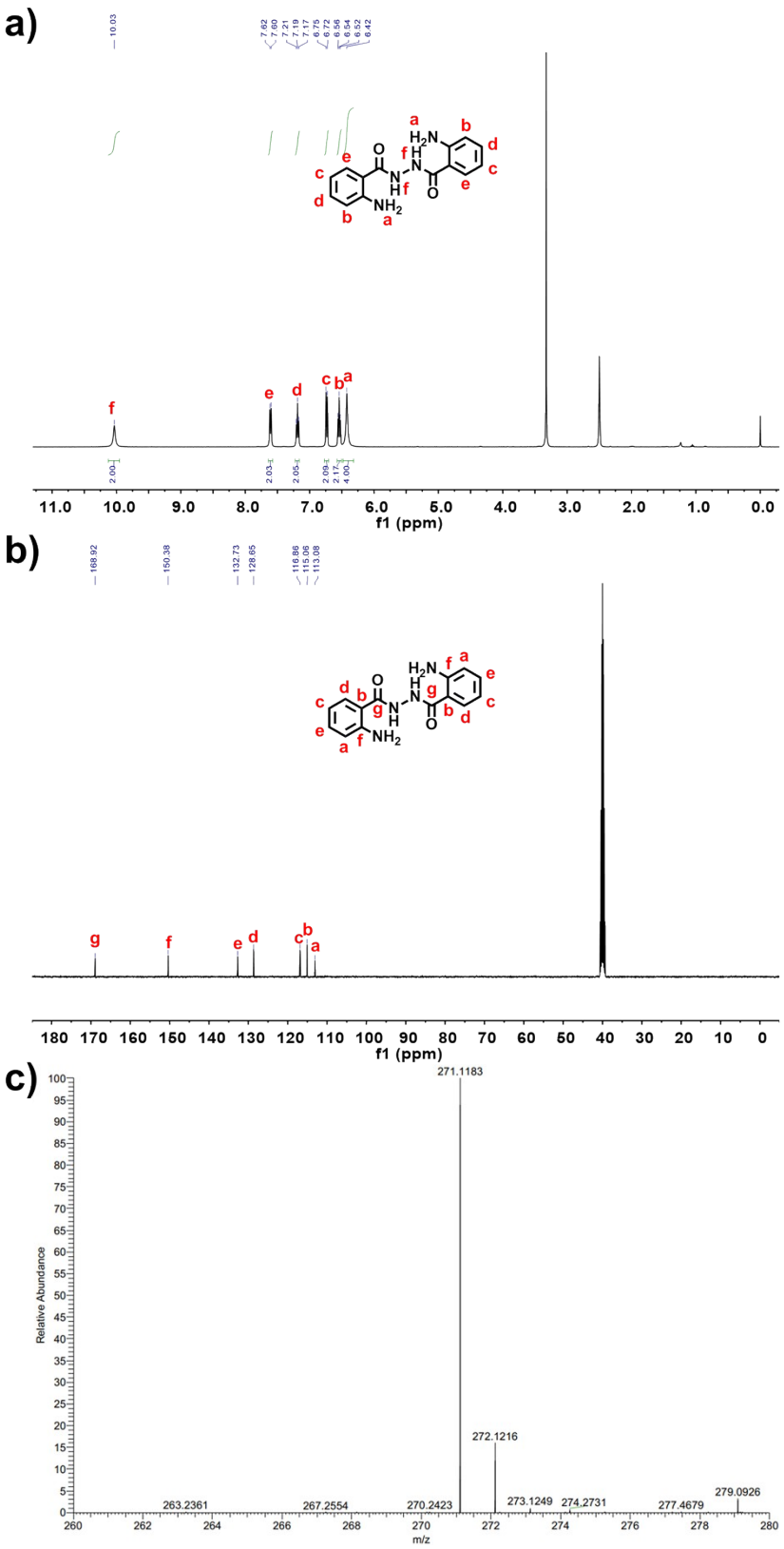

Fig. S1 a) ^{1}H NMR, b) ^{13}C NMR, c) HRMS spectra of AABH. HRMS (ESI): *m/z* $[M+H]^+$ calcd for $C_{14}H_{14}N_4O_2$ 271.1190; found, 271.1183.

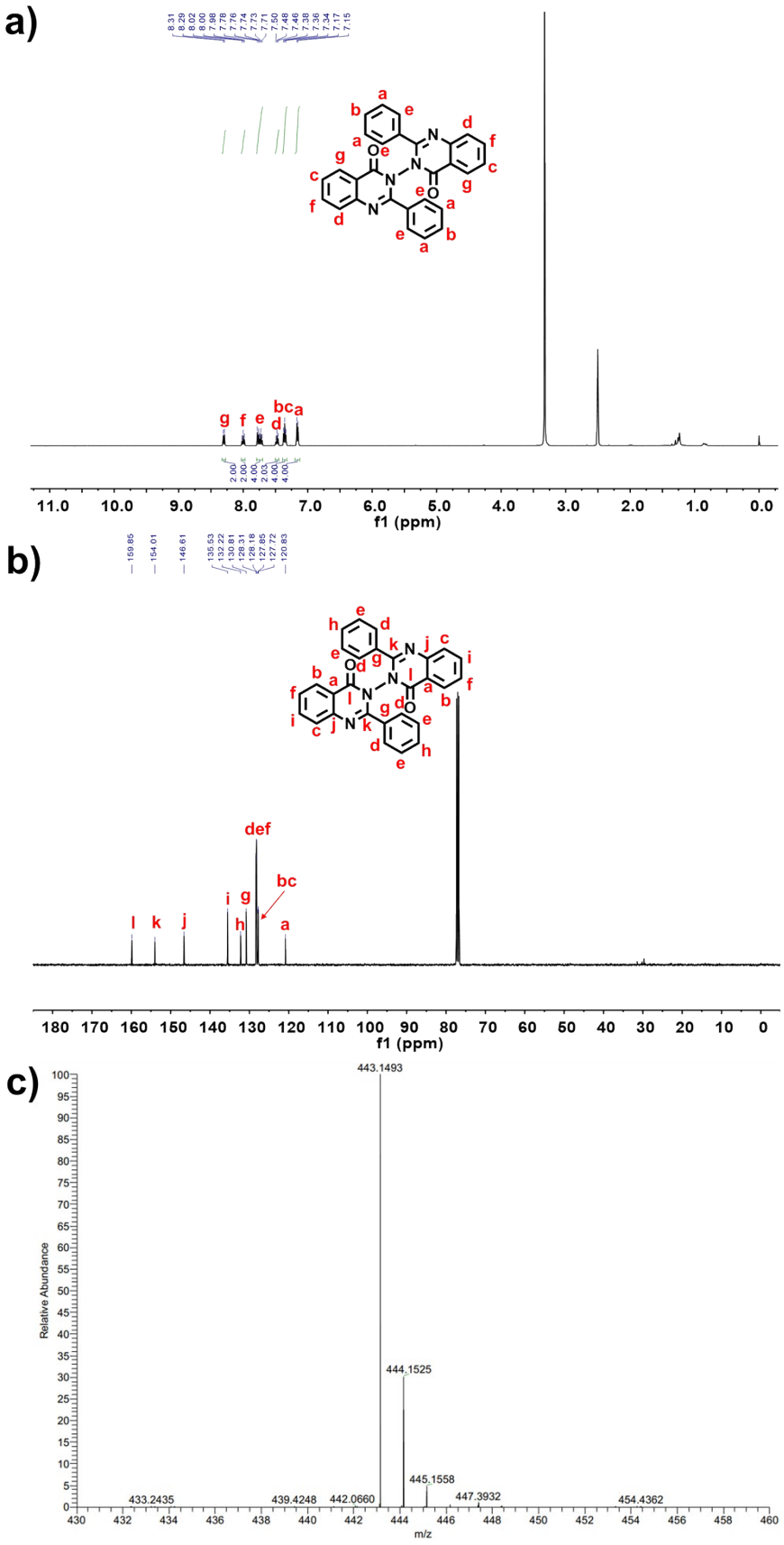

Fig. S2 a) ^{1}H NMR, b) ^{13}C NMR, c) HRMS spectra of the model compound. HRMS (ESI): *m/z* $[M+H]^+$ calcd for $C_{28}H_{18}N_4O_2$ 443.1503; found, 443.1493.

Table S1 Crystal data and structure refinement for AABH.

Identification code	CCDC 2544533
Empirical formula	C7H7N2O
Formula weight	135.15
Temperature/K	294.76(11)
Crystal system	monoclinic
Space group	$P_{21/c}$
a/Å	12.926(3)
b/Å	5.3094(11)
c/Å	9.688(2)
α/°	90
β/°	111.73(3)
γ/°	90
Volume/Å^3	617.7(3)
Z	4
ρ_{calc}g/cm^3	1.453
μ/mm^{-1}	0.101
F(000)	284.0
Crystal size/mm^3	0.12 × 0.1 × 0.05
Radiation	Mo Kα (λ = 0.71073)
2Θ range for data collection/°	8.394 to 58.794
Index ranges	-17 ≤ h ≤ 17, -4 ≤ k ≤ 6, -13 ≤ l ≤ 13
Reflections collected	4402
Independent reflections	1492 [R_{int} = 0.0295, R_{sigma} = 0.0420]
Data/restraints/parameters	1492/0/99
Goodness-of-fit on F^2	0.858
Final R indexes [I>=2σ (I)]	R_1 = 0.0530, wR_2 = 0.1487
Final R indexes [all data]	R_1 = 0.0824, wR_2 = 0.1874
Largest diff. peak/hole / e Å^{-3}	0.22/-0.27

Table S2 Crystal data and structure refinement for model compound.

Identification code	CCDC 2544364
Empirical formula	$C_{28}H_{18}N_4O_2$
Formula weight	442.46
Temperature/K	200.00(10)
Crystal system	orthorhombic
Space group	P_{bca}
a/Å	16.0275(13)
b/Å	14.7197(16)
c/Å	18.5097(19)
α/°	90
β/°	90
γ/°	90
Volume/Å^3	4366.8(7)
Z	8
ρ_{calc}g/cm^3	1.346
μ/mm^{-1}	0.087
F(000)	1840.0
Crystal size/mm^3	0.22 × 0.15 × 0.1
Radiation	Mo Kα (λ = 0.71073)
2Θ range for data collection/°	6.726 to 58.802
Index ranges	-20 ≤ h ≤ 20, -18 ≤ k ≤ 20, -25 ≤ l ≤ 25
Reflections collected	36100
Independent reflections	5533 [R_{int} = 0.0836, R_{sigma} = 0.0659]
Data/restraints/parameters	5533/0/307
Goodness-of-fit on F^2	1.032
Final R indexes [I>=2σ (I)]	R_1 = 0.0712, wR_2 = 0.1902
Final R indexes [all data]	R_1 = 0.1512, wR_2 = 0.2517
Largest diff. peak/hole / e Å^{-3}	0.39/-0.29

3. Characterization of AABH-TFBT-COF

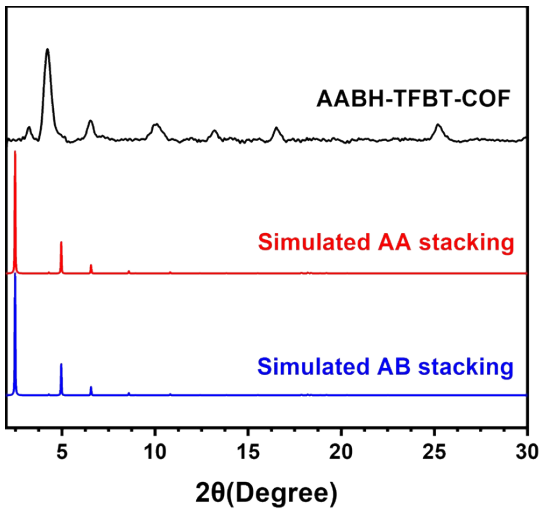

Fig. S3. The PXRD patterns of experimental data and simulated AA and AB stacking of **AABH-TFBT-COF**.

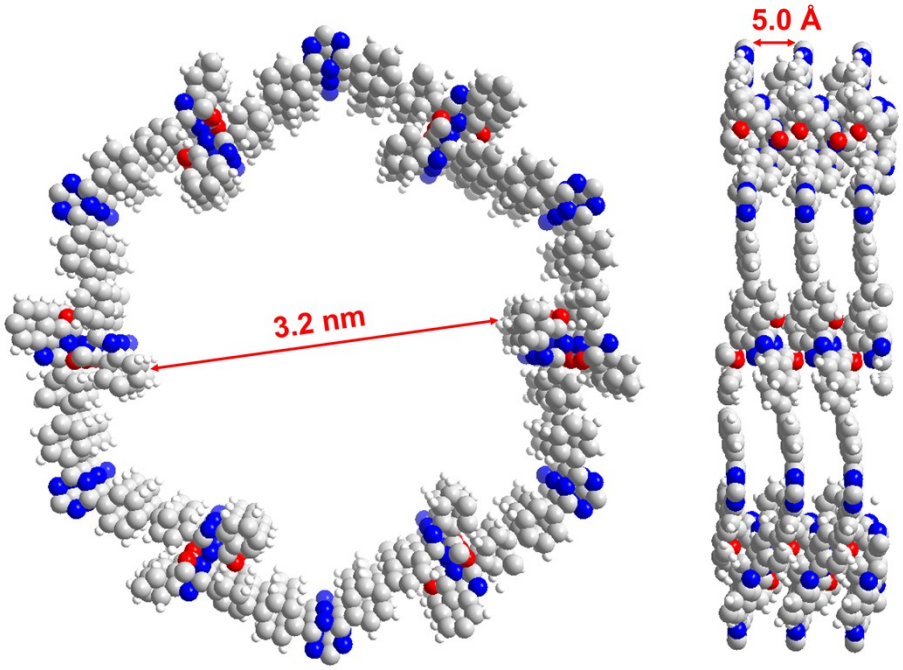

Fig. S4. The eclipsed structures of AA stacking mode for **AABH-TFBT-COF**.

Table S3. Fractional atomic coordinates for the unit cell of **AABH-TFBT-COF.**
AABH-TFBT-COF AA stacking mode, space group: P_3
a = 41.1629 Å, b = 41.1629 Å, c = 5.0134 Å

Atom	x/a	y/b	z/c	Atom	x/a	y/b	z/c
C1	1.27635	-0.54113	0.03791	C38	-0.92129	-0.48979	-0.92129
C2	1.26083	-0.57904	-0.02587	C39	-0.89607	-0.48661	-0.89607
C3	1.23068	-0.60656	0.12204	C40	-0.85824	-0.42543	-0.85824
C4	1.2175	-0.59588	0.34251	C41	-0.84477	-0.36579	-0.84477

C5	1.23261	-0.55783	0.4045	C42	-0.86954	-0.38209	-0.86954
C6	1.26206	-0.53009	0.25199	C43	-0.90735	-0.44373	-0.90735
C7	1.26661	-0.43762	0.40209	C44	-0.80576	-0.27002	-0.80576
C8	1.25266	-0.47603	0.36604	C45	-0.79009	-0.08571	-0.79009
C9	1.27709	-0.48971	0.30983	C46	-0.75399	0.01357	-0.75399
C10	1.31584	-0.46433	0.29876	C47	-0.73271	-0.06876	-0.73271
C11	1.32983	-0.42596	0.33627	C48	-0.74835	-0.25065	-0.74835
C12	1.30533	-0.41206	0.38401	C49	-0.78444	-0.35219	-0.78444
C13	1.31992	-0.37108	0.40173	C50	-0.69471	0.0388	-0.69471
N14	1.35747	-0.34664	0.40114	H51	-0.52042	-0.08563	-0.52042
C15	1.21298	-0.75827	-0.36983	H52	-0.5869	-0.19578	-0.5869
C16	1.24208	-0.74292	-0.18309	H53	-0.6171	0.45786	-0.6171
C17	1.2494	-0.71076	-0.04085	H54	-0.54983	0.57141	-0.54983
C18	1.22749	-0.69404	-0.08517	H55	-0.42792	0.43941	-0.42792
C19	1.19877	-0.70884	-0.27515	H56	-0.49491	0.37359	-0.49491
C20	1.1912	-0.74145	-0.41515	H57	-0.47416	0.25933	-0.47416
C21	1.17566	-0.69069	-0.30094	H58	-0.40713	0.32179	-0.40713
N22	1.17885	-0.66493	-0.11273	H59	-0.78341	-0.47785	-0.78341
N23	1.14688	-0.66188	-0.04214	H60	-0.756	-0.14806	-0.756
C24	1.14964	-0.62722	-0.017	H61	-0.69891	0.10365	-0.69891
C25	1.12465	-0.62238	0.16871	H62	-0.75459	-0.55281	-0.75459
C26	1.13135	-0.58691	0.25054	H63	-0.56156	0.17045	-0.56156
C27	1.10819	-0.58418	0.44266	H64	-0.55688	0.50809	-0.55688
C28	1.0783	-0.61668	0.55187	H65	-0.61449	0.70116	-0.61449
C29	1.07142	-0.65199	0.46849	H66	-0.67704	0.55269	-0.67704
C30	1.09481	-0.65476	0.27844	H67	-0.90572	-0.52398	-0.90572
N31	1.23572	-0.66035	0.05115	H68	-0.83961	-0.41979	-0.83961
O32	1.15276	-0.69966	-0.47956	H69	-0.86006	-0.33547	-0.86006
O33	1.17324	-0.60032	-0.14052	H70	-0.92591	-0.44495	-0.92591
N34	1.08786	-0.69063	0.18882	H71	-0.80591	-0.01521	-0.80591
C35	1.21378	-0.64607	0.04009	H72	-0.74225	0.14857	-0.74225
N36	1.03748	-0.97607	-0.51828	H73	-0.73247	-0.31536	-0.73247
C37	1.01367	-0.9622	-0.5192	H74	-0.79564	-0.49536	-0.79564

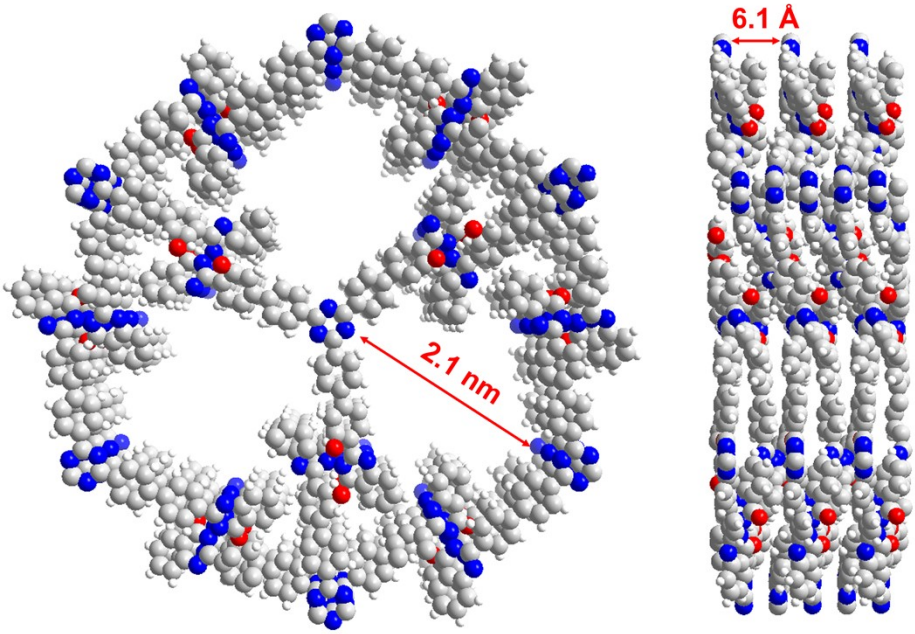

Fig. S5. The staggered structures of AB stacking mode for **AABH-TFBT-COF**.

Table S4. Fractional atomic coordinates for the unit cell of **AABH-TFBT-COF.**
AABH-TFBT-COF AB stacking mode, space group: P_{63}
a = 41.1340 Å, *b* = 41.1340 Å, *c* = 6.1221 Å

Atom	x/a	y/b	z/c	Atom	x/a	y/b	z/c
C1	1.28325	-0.54653	-0.03412	C38	1.03091	-0.92071	0.31597
C2	1.27008	-0.58504	-0.04574	C39	1.06994	-0.89647	0.30021
C3	1.23349	-0.61129	0.02145	C40	1.08476	-0.85811	0.26045
C4	1.21048	-0.59794	0.10452	C41	1.06084	-0.84316	0.23499
C5	1.22354	-0.5592	0.11315	C42	1.02197	-0.86707	0.26099
C6	1.26025	-0.53294	0.04589	C43	1.0072	-0.90535	0.30082
C7	1.26559	-0.43758	0.02092	C44	1.07592	-0.80351	0.16591
C8	1.2514	-0.47648	0.01455	C45	1.10926	-0.77419	0.25534
C9	1.2748	-0.49157	0.05847	C46	1.12349	-0.73703	0.18429
C10	1.31265	-0.46664	0.11117	C47	1.10517	-0.72888	0.01771
C11	1.32689	-0.42782	0.11539	C48	1.07176	-0.75821	-0.0697
C12	1.30362	-0.41272	0.06959	C49	1.05731	-0.79499	0.00312
C13	1.31909	-0.37132	0.07098	C50	1.12004	-0.69052	-0.07287
N14	1.35687	-0.34744	0.07088	H51	1.31132	-0.52739	-0.0925
C15	1.22812	-0.77032	-0.09629	H52	1.28842	-0.59443	-0.11207
C16	1.25914	-0.74516	0.02789	H53	1.18232	-0.61741	0.16026
C17	1.26414	-0.70989	0.08132	H54	1.20503	-0.54971	0.17403
C18	1.2382	-0.69965	0.00941	H55	1.24685	-0.42696	-0.01606
C19	1.20744	-0.72451	-0.11757	H56	1.22226	-0.49464	-0.02947
C20	1.20225	-0.7601	-0.16958	H57	1.33139	-0.47713	0.15086
C21	1.18131	-0.71196	-0.1897	H58	1.3562	-0.40963	0.15591
N22	1.18596	-0.67813	-0.11719	H59	1.22422	-0.79768	-0.13609

N23	1.15792	-0.6687	-0.16276	H60	1.27943	-0.75287	0.08178
C24	1.16609	-0.63896	-0.29969	H61	1.28829	-0.69047	0.17662
C25	1.13971	-0.62468	-0.31648	H62	1.17842	-0.7798	-0.26617
C26	1.14872	-0.59124	-0.42581	H63	1.176	-0.57445	-0.49945
C27	1.12254	-0.57904	-0.43614	H64	1.12949	-0.55329	-0.52105
C28	1.08748	-0.6	-0.33594	H65	1.06721	-0.59057	-0.34442
C29	1.07868	-0.633	-0.22355	H66	1.05156	-0.6491	-0.14557
C30	1.10496	-0.64508	-0.21211	H67	1.08907	-0.90731	0.31077
N31	1.24417	-0.66294	0.05441	H68	1.11481	-0.84048	0.23976
O32	1.15538	-0.73174	-0.31122	H69	1.00285	-0.85628	0.24588
O33	1.19534	-0.62404	-0.40338	H70	0.97702	-0.92307	0.31284
N34	1.09603	-0.67895	-0.09925	H71	1.12415	-0.78013	0.38029
C35	1.22054	-0.65207	-0.00266	H72	1.149	-0.71483	0.25651
N36	1.03769	-0.97701	0.33248	H73	1.05721	-0.75278	-0.19916
C37	1.01484	-0.96197	0.33316	H74	1.03199	-0.81697	-0.07225

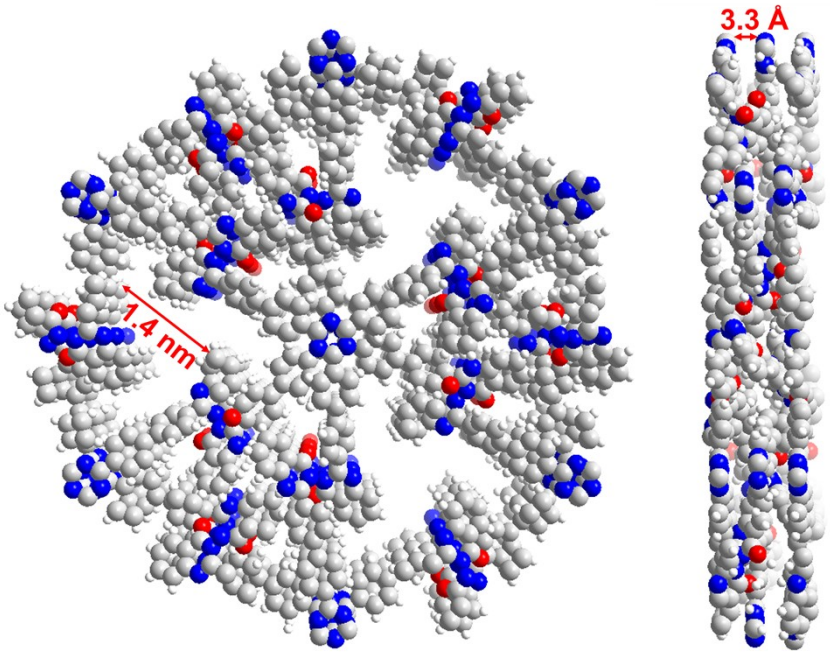

Fig. S6. The staggered structures of ABC stacking mode for **AABH-TFBT-COF**.

Table S5. Fractional atomic coordinates for the unit cell of **AABH-TFBT-COF**
AABH-TFBT-COF ABC stacking mode, space group: R_3
a = 41.2891 Å, b = 41.2891 Å, c = 6.6283 Å
$\alpha = \beta$ = 90.0000°, γ = 120.0000°, R_{wp} = 6.33 % and R_p = 4.17 %

Atom	x/a	y/b	z/c	Atom	x/a	y/b	z/c
C1	1.25476	-0.54255	-0.07933	C38	1.02413	-0.92279	0.05481
C2	1.23716	-0.57996	-0.13918	C39	1.06189	-0.89613	0.02109
C3	1.20749	-0.60782	-0.02657	C40	1.07363	-0.85785	0.01537

C4	1.19625	-0.5975	0.15095	C41	1.04796	-0.84523	0.04569
C5	1.21373	-0.55972	0.21029	C42	1.0102	-0.87217	0.08095
C6	1.24329	-0.53181	0.09557	C43	0.99843	-0.91038	0.08329
C7	1.25884	-0.43576	0.24135	C44	1.0602	-0.80438	0.04072
C8	1.24121	-0.47456	0.21072	C45	1.09583	-0.77701	0.11037
C9	1.26209	-0.49145	0.15291	C46	1.10633	-0.73895	0.11259
C10	1.30117	-0.46888	0.13626	C47	1.08156	-0.72743	0.04339
C11	1.3188	-0.43026	0.16885	C48	1.04619	-0.75457	-0.02662
C12	1.29781	-0.41302	0.21719	C49	1.03583	-0.79238	-0.03066
C13	1.31631	-0.3715	0.23083	C50	1.09176	-0.6874	0.03967
N14	1.3543	-0.35018	0.2303	H51	1.27696	-0.5218	-0.17286
C15	1.17187	-0.7639	-0.4447	H52	1.24631	-0.58714	-0.27677
C16	1.20829	-0.74491	-0.36763	H53	1.1738	-0.61853	0.24205
C17	1.22132	-0.71074	-0.26778	H54	1.20444	-0.55236	0.34663
C18	1.1979	-0.69553	-0.24524	H55	1.24179	-0.42347	0.27894
C19	1.16179	-0.71404	-0.32662	H56	1.21106	-0.49109	0.2236
C20	1.14854	-0.74861	-0.42363	H57	1.31814	-0.48107	0.09476
C21	1.13822	-0.69708	-0.29431	H58	1.34883	-0.41378	0.14979
N22	1.14993	-0.66756	-0.16209	H59	1.16167	-0.79056	-0.51965
N23	1.12329	-0.65939	-0.07813	H60	1.22632	-0.75679	-0.38413
C24	1.12598	-0.62527	-0.11496	H61	1.24943	-0.69627	-0.20722
C25	1.10228	-0.61445	-0.00072	H62	1.12012	-0.76394	-0.47913
C26	1.10797	-0.57797	-0.00414	H63	1.13069	-0.55625	-0.09053
C27	1.08435	-0.56941	0.10622	H64	1.08866	-0.54131	0.10326
C28	1.05501	-0.59718	0.21928	H65	1.03629	-0.59073	0.30155
C29	1.04999	-0.63324	0.22752	H66	1.02749	-0.65445	0.31687
C30	1.07382	-0.6418	0.119	H67	1.08232	-0.90491	-0.00269
N31	1.21093	-0.66061	-0.14316	H68	1.10277	-0.83823	-0.01557
O32	1.10799	-0.70993	-0.37858	H69	0.9896	-0.86384	0.10978
O33	1.14788	-0.60407	-0.24096	H70	0.96915	-0.93024	0.10985
N34	1.06893	-0.67862	0.12737	H71	1.11541	-0.78501	0.16692
C35	1.18917	-0.64704	-0.10123	H72	1.13371	-0.71855	0.16853
N36	1.03291	-0.9774	0.06099	H73	1.02643	-0.74649	-0.07874
C37	1.01149	-0.96333	0.06114	H74	1.00858	-0.81217	-0.09046

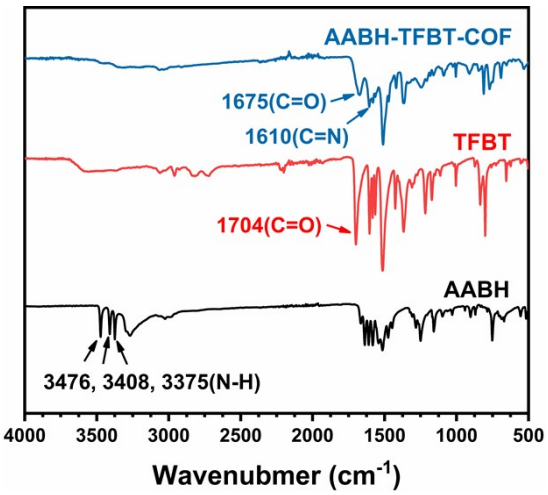

Fig. S7. FTIR spectra of **AABH-TFBT-COF** and monomers.

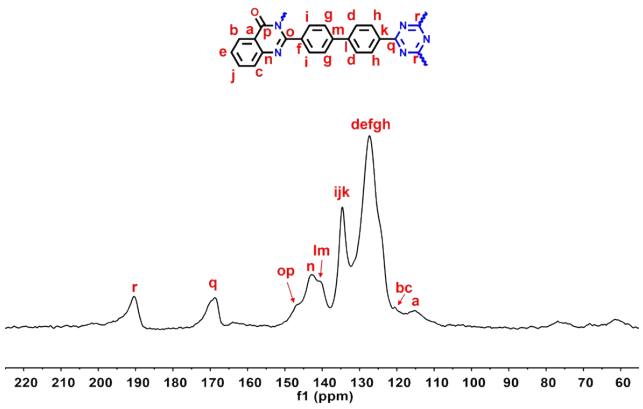

Fig. S8. ^{13}C CP-MAS solid-state NMR spectrum of **AABH-TFBT-COF**.

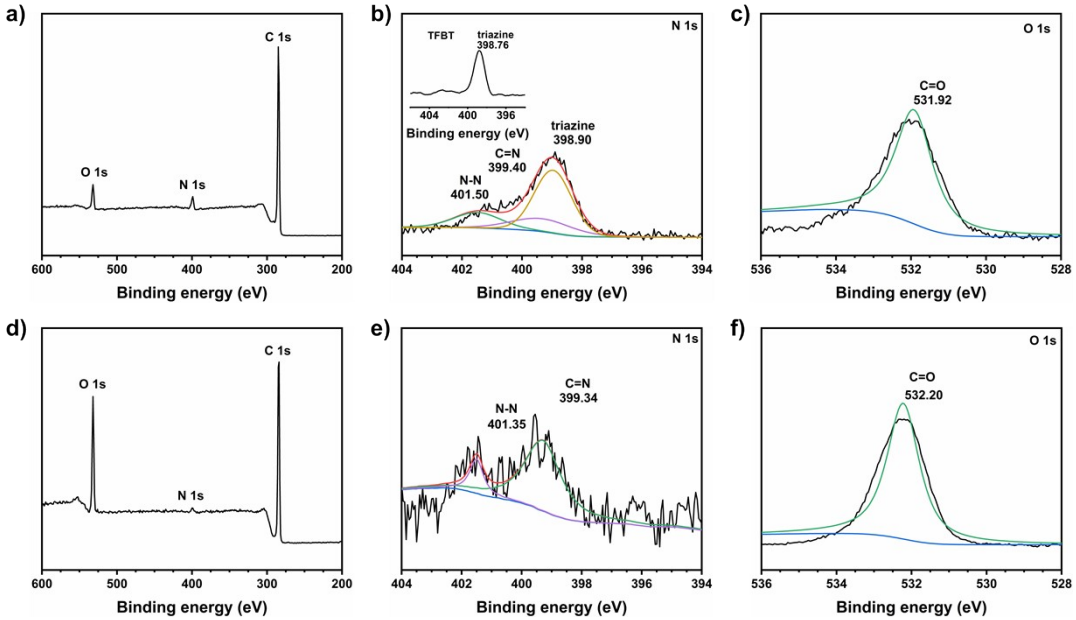

Fig. S9. XPS spectra of **AABH-TFBT-COF** (a-c) and the model compound (d-f). (a, d) Survey scans. (b) N 1s of the COF: triazine N (398.90 eV, inset: TFBT monomer), C=N (399.40 eV), N-N (401.50 eV). (e) N 1s of the model compound: C=N (399.34 eV), N-N (401.35 eV). (c, f) O 1s (C=O). The consistent N-N peak positions confirm the preservation of the heterocycle-embedded N-N linkage in the COF.

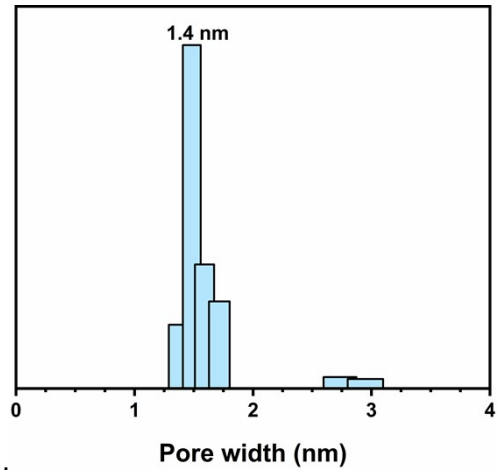

Fig. S10. The pore size distribution of **AABH-TFBT-COF**

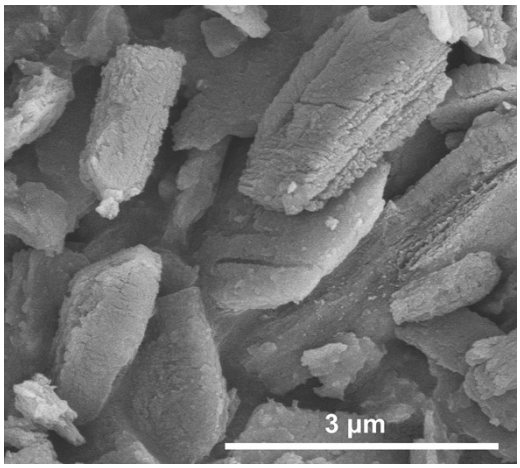

Fig. S11. SEM image of **AABH-TFBT-COF**.

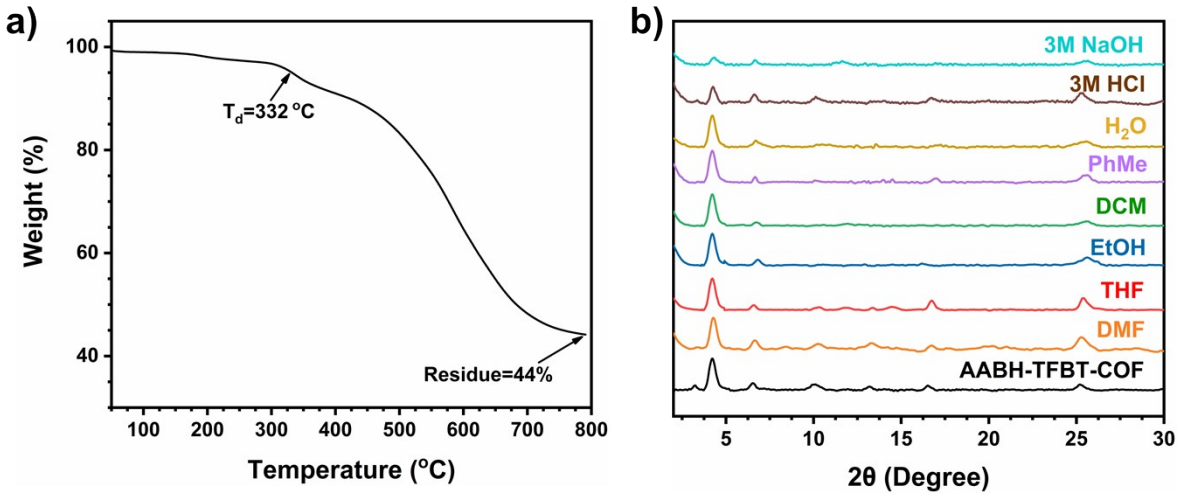

Fig. S12. a) TGA curve of **AABH-TFBT-COF**. b) PXRD patterns of **AABH-TFBT-COF** after soaking in different media for 24 h.

4. Characterization of Pd@AABH-TFBT-COF

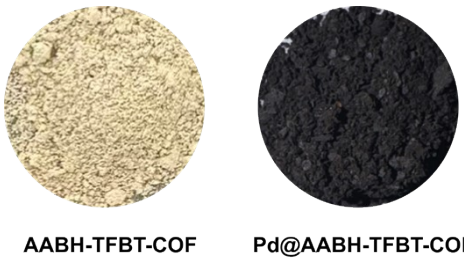

Fig. S13. Digital photograph of **AABH-TFBT-COF** and **Pd@AABH-TFBT-COF.**

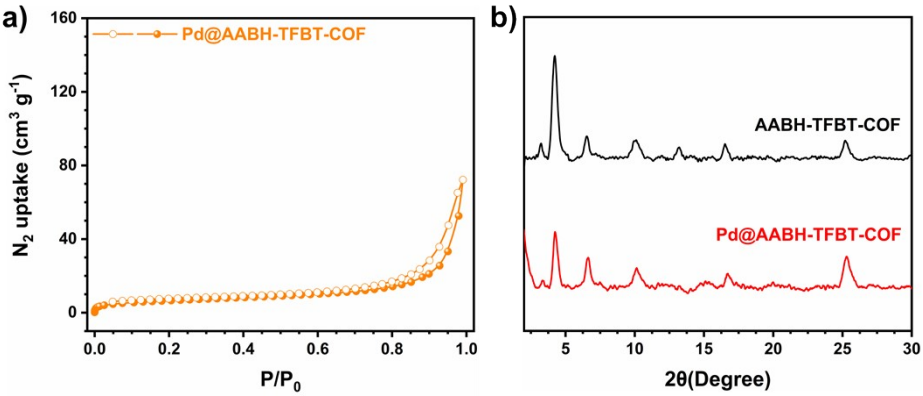

Fig. S14. a) N_2 adsorption-desorption isotherm at 77 K of **Pd@AABH-TFBT-COF** and b) PXRD patterns of **AABH-TFBT-COF** and **Pd@AABH-TFBT-COF**

5. Pd@AABH-TFBT-COF- catalyzed model reaction

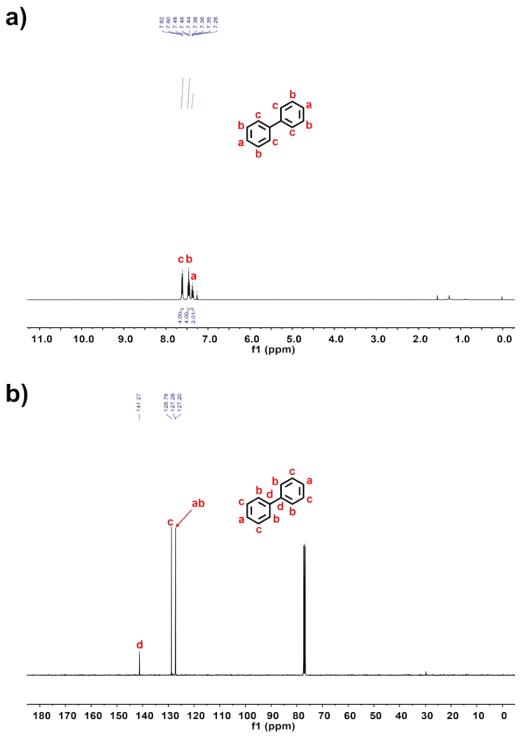

Fig. S15. Characterization of biphenyl. a) ^{1}H-NMR (400 MHz, $CDCl_3$, ppm): δ=7.62 (m, 4H), 7.46 (m, 4H), 7.36 (m, 2H). b) ^{13}C-NMR (100 MHz, $CDCl_3$, ppm): δ=141.27, 128.78, 127.28. 127.20.

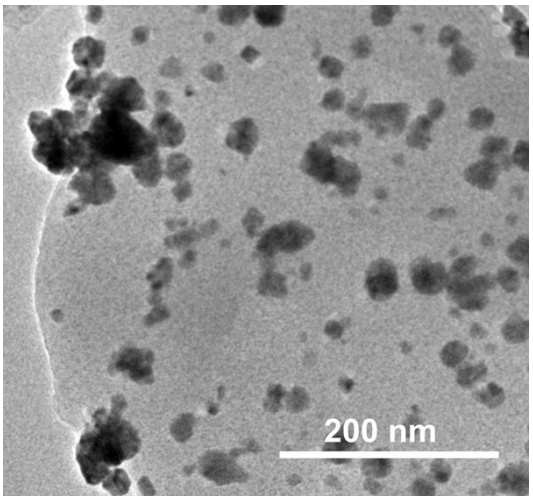

Fig. S16. HRTEM image of **Pd@AABH-TFBT-COF** obtained with hydrazine hydrate as the reductant instead of $NaBH_4$, showing large Pd NPs of ~35 nm (see Section 1.5 for synthesis details). The corresponding catalytic activity is significantly lower (68 % yield, Table S6, entry 10), highlighting the importance of small Pd NPs for high performance.

Table S6. Optimization of reaction conditions for Suzuki-Miyaura coupling reaction catalyzed by **Pd@AABH-TFBT-COF**[a]

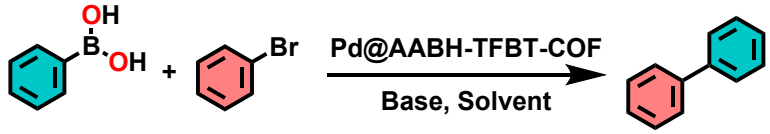

Entry	Base	Solvent	Pd (%)	T (°C)	t (h)	Yield (%)[b]
1	K_2CO_3	DMF/H_2O	0.5	50	5	99
2	K_2CO_3	DMF	0.5	50	5	55
3	K_2CO_3	H_2O	0.5	50	5	14
4	K_2CO_3	Toluene	0.5	50	5	68
5	K_2CO_3	Toluene/H_2O	0.5	50	5	27
6	K_2CO_3	THF	0.5	50	5	15
7	K_2CO_3	THF/H_2O	0.5	50	5	24
8	K_2CO_3	Dioxane	0.5	50	5	18
9	K_2CO_3	Dioxane/H_2O	0.5	50	5	17
10[c]	K_2CO_3	DMF/H_2O	0.5	50	5	68

[a]Reaction conditions: phenyl boronic acid (1 mmol), aryl halide (1.1 mmol), **Pd@AABH-TFBT-COF** (3.3 mg, 0.5 mol% Pd loading), K_2CO_3 (1.5 mmol), DMF/H_2O (1.5 mL/1.5 mL),50 °C. [b]Isolated yield. [c]Catalysis by **Pd@AABH-TFBT-COF** with larger Pd NPs (~35 nm)

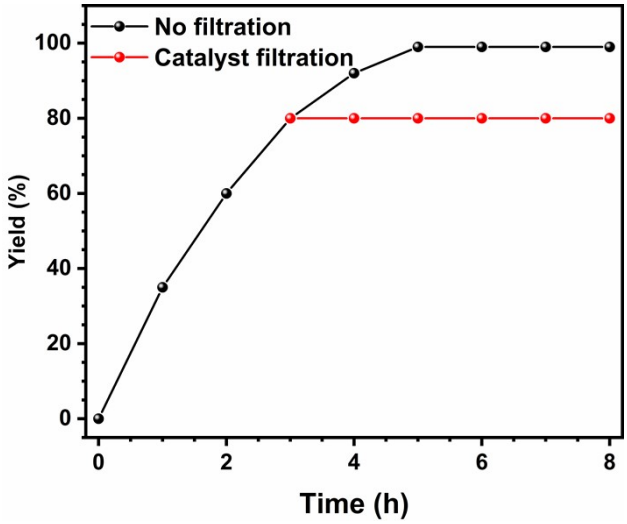

Fig. S17. Reaction time examination and leaching test for model reaction.

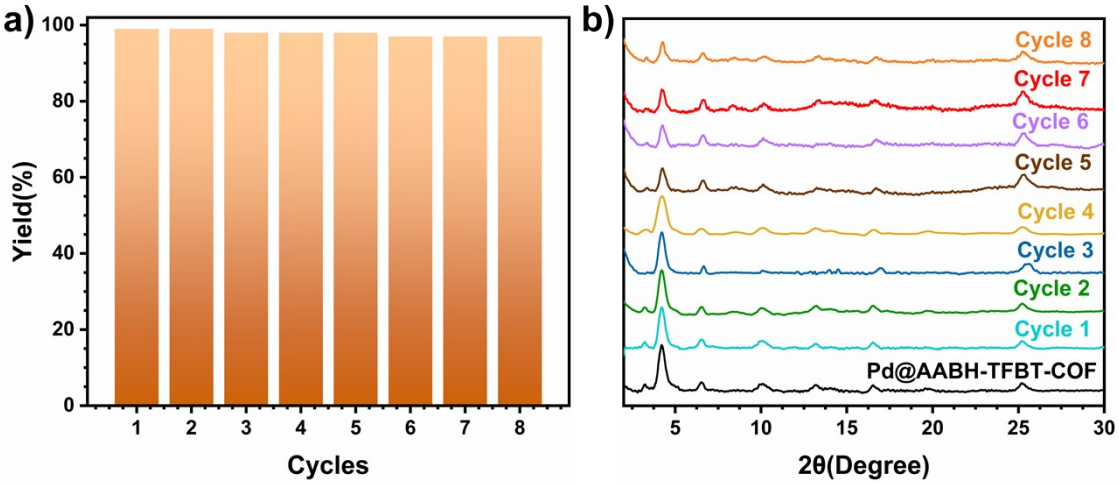

Fig. S18. a) Catalytic cycles for model reaction. b) PXRD patterns of **Pd@AABH-TFBT-COF** before and after eight cycles.

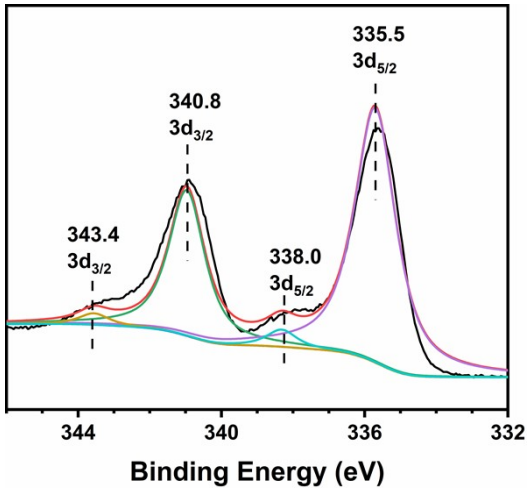

Fig. S19. Pd 3d XPS spectrum of the **Pd@AABH-TFBT-COF** catalyst after eight catalytic cycles.

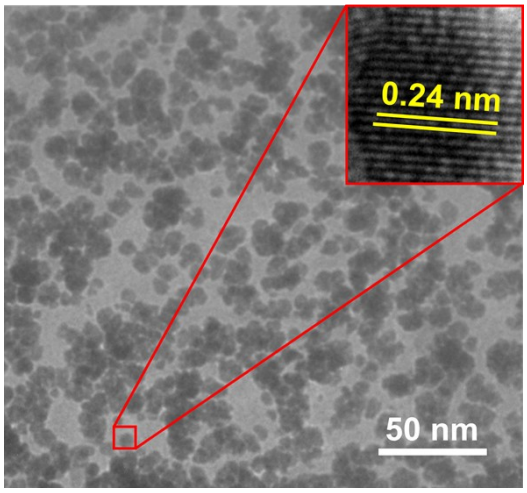

Fig. S20. HRTEM image of **Pd@AABH-TFBT-COOH** after eight catalytic cycles.

Table S7. Comparison with reported Pd@COFs catalysts in the Suzuki–Miyaura coupling of bromobenzene and phenylboronic acid.

Entry	Catalyst	Pd Valence	T (°C)	Time (h)	Yield (%)	Recyclability (runs)	TON	TOF (h^{-1})	Ref.
1	Pd@COF-TB	Pd^{2+}	95	8	93	8	211	26	[2]
2	Pd@-COF-QA	Pd^{0}	50	6	99	10	59	10	[3]
3	3D-Pd-NHC-COF	Pd^{2+}	120	24	92	5	11.7	4.7	[4]
4	Pd/COF-LZU-1	Pd^{2+}	150	3	97	4	192	64	[5]
5	Pd@MC-Tab-Dva COF	Pd^{2+}	150	2	99	4	50	25	[6]
6	$ZnFe_2O_4$@PDACOF@Pd	Pd^{0}	50	1	99	5	59	59	[7]
7	Pd/Bth-Tp-COF	Pd^{2+}	100	0.3	99	5	317	951	[8]
8	Pd@TTA-DFB	Pd^{2+}	150	2	97	-	194	97	[9]
9	Pd(II)@SP-3D-COF-BPY	Pd^{2+}	70	2	98	4	196	98	[10]
10	Pd/COF-SMC2	Pd^{2+}	80	1	96	3	192	192	[11]
11	CS/ZIF-8@COFa-4@Pd	Pd^{0}	80	4	99	5	18	4.5	[12]
12	Pd/COF-DB	Pd^{2+}	80	0.5	99	4	163.4	326.7	[13]
13	MCM@Pd@COF	Pd^{0}	90	2	97	8	650	325	[14]
14	Pd-NP@Tfpa-Od	Pd^{0}	90	24	99	3	198	8.3	[15]
15	Pd@PDPP-TBP	Pd^{0}	40	2	99	5	171	85	[16]
16	Pd@COF-TFP _TzPy	Pd^{2+}	RT	3	91	4	160	53	[17]

17	Pd/AntCOF	Pd^0	RT	12	97	4	24	2	[18]
18	TAPB-BTCA	Pd^{2+}	80	2	51	-	102	51	[19]
19	PdNPs@UCOF-SH	Pd^0	80	2	99	8	132	66	[20]
20	Pd/DMTP-TPB	Pd^{2+}	RT	1	99	3	99	99	[21]
21	Pd/H_2P-Bph-COF	Pd^{2+}	110	1.5	97.5	4	195	130	[22]
22	Pd@TU-COF	Pd^{2+}	RT	4	99	10	182	46	[23]
23	IHP-Br-Pd-NPs	Pd^0	100	6	100	9	27	4.6	[24]
24	Pd@AABH-TFBT-COF	Pd^0	50	5	99	8	198	39.6	This work

6. Scope of Pd@AABH-TFBT-COF-catalyzed Suzuki-Miyaura coupling reaction.

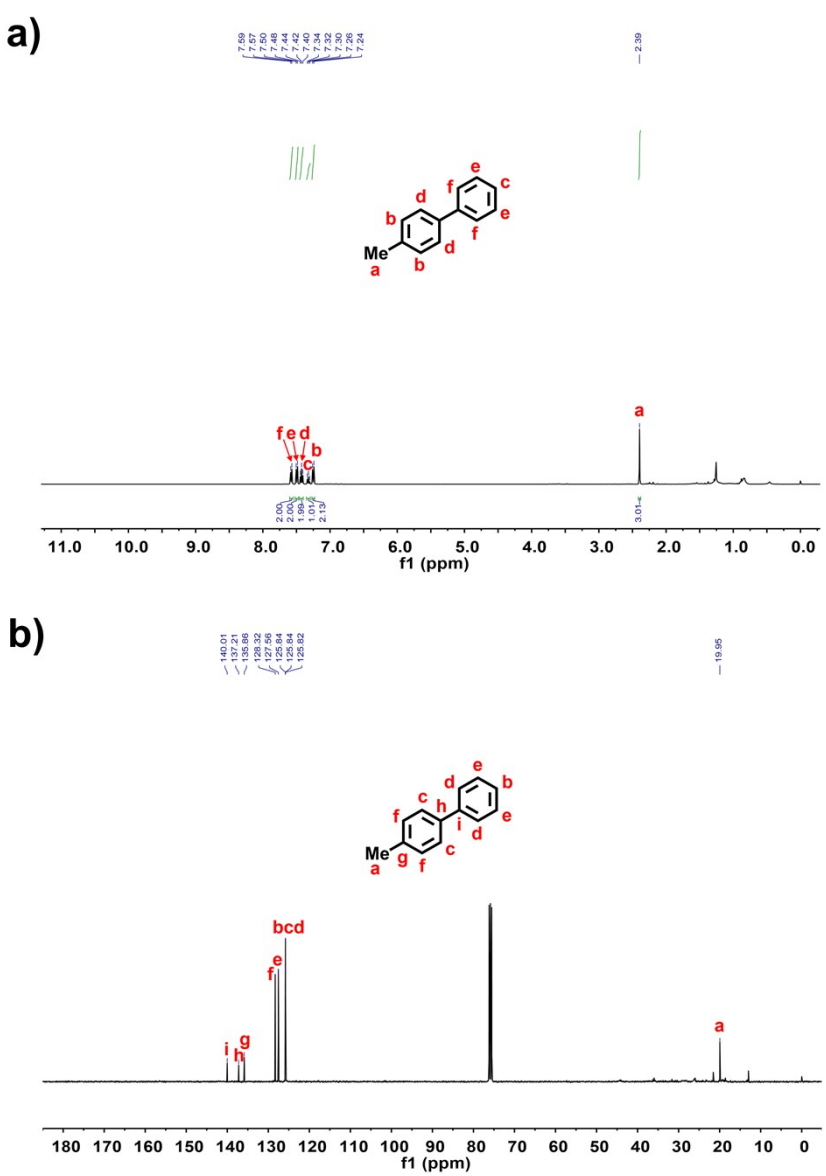

Fig. S21. Characterization of 4-phenyltoluene. a) ^{1}H-NMR (400 MHz, $CDCl_3$, ppm): δ=7.57 (d, J=8 Hz, 2H), 7.48 (d, J=8 Hz, 2H), 7.42 (t, J=8 Hz, 2H), 7.32 (t, J=8 Hz, 2H), 7.24 (d, J=8 Hz, 2H), 2.39 (s, 3H). b) ^{13}C-NMR (100 MHz, $CDCl_3$, ppm): δ=140.01, 137.21,135.86, 128.32,127.56, 125.84, 125.83, 125.82, 19.95.

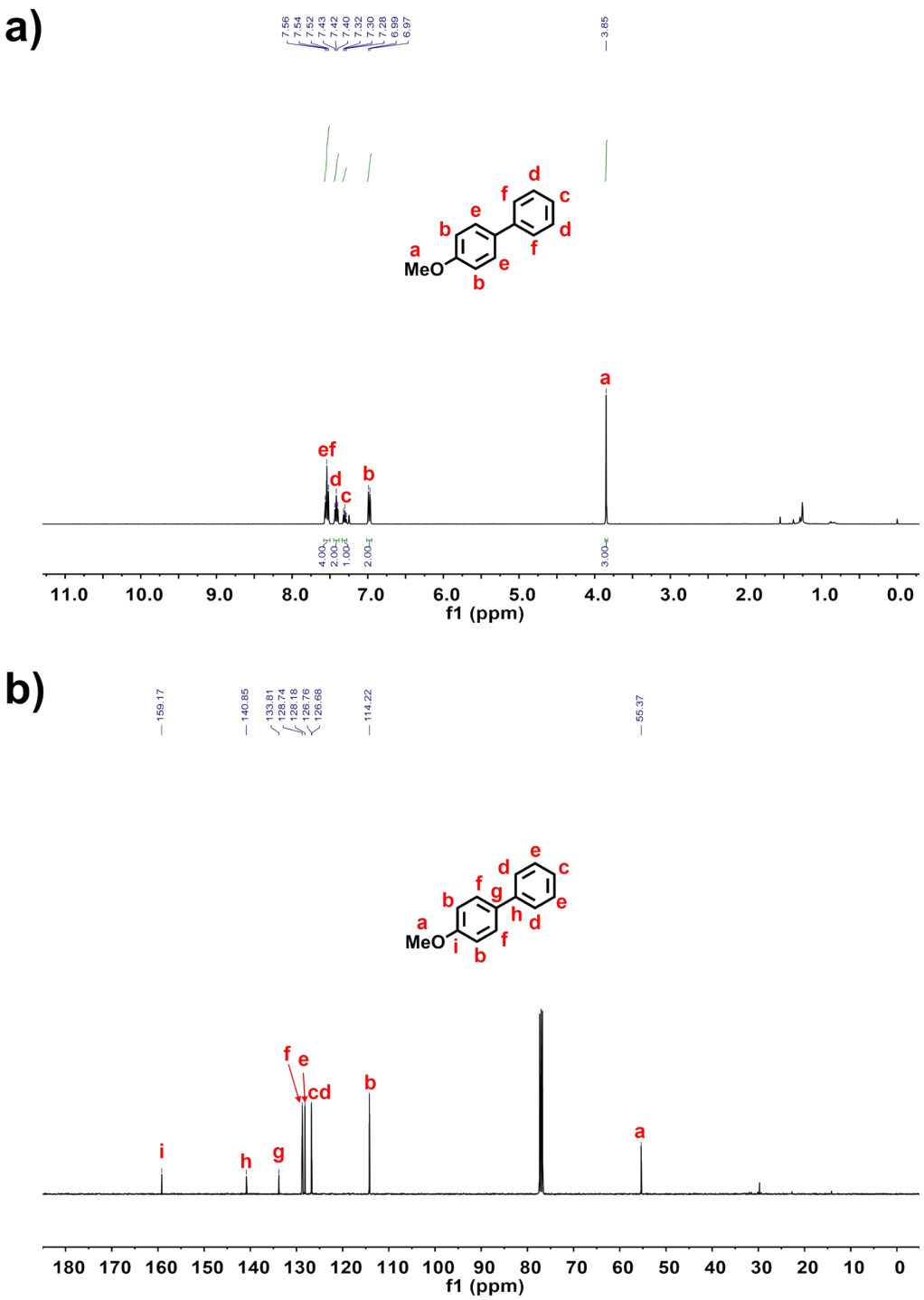

Fig. S22. Characterization of 4-methoxybiphenyl. a) ^{1}H-NMR (400 MHz, $CDCl_3$, ppm): δ=7.54 (t, J=8 Hz, 4H), 7.42 (t, J=8 Hz, 2H), 7.30 (t, J=8 Hz, 1H), 6.97 (d, J=8 Hz, 2H), 3.85 (s, 3H). b) ^{13}C-NMR (100 MHz, $CDCl_3$, ppm): δ=159.17, 140.85, 133.81, 128.74, 128.18, 126.78, 126.68, 114.22, 55.37.

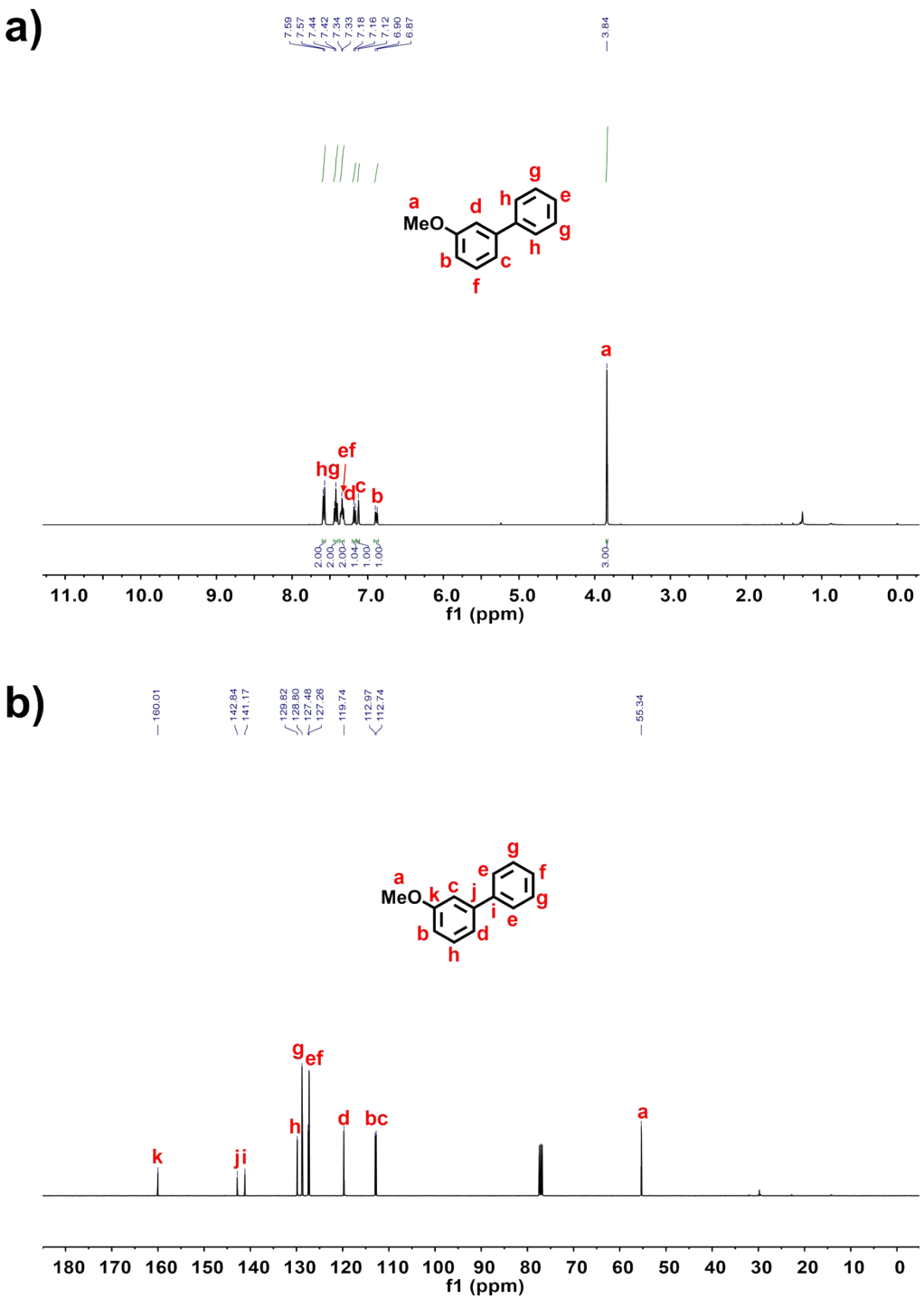

Fig. S23. Characterization of 3-methoxybiphenyl. a) ^{1}H-NMR (400 MHz, $CDCl_3$, ppm): δ=7.57 (d, J=8 Hz, 2H), 7.42 (t, J=8 Hz, 2H), 7.43 (m, 2H), 7.16 (d, J=8 Hz, 1H), 7.12 (s, 1H), 6.88 (dd, J_1=8 Hz, J_2=4 Hz,1H), 3.84 (s, 3H). b) ^{13}C-NMR (100 MHz, $CDCl_3$, ppm): δ=160.01, 142.84, 141.17, 129.82, 128.80, 127.48, 127.26, 119.74, 112.97, 112.74, 55.34.

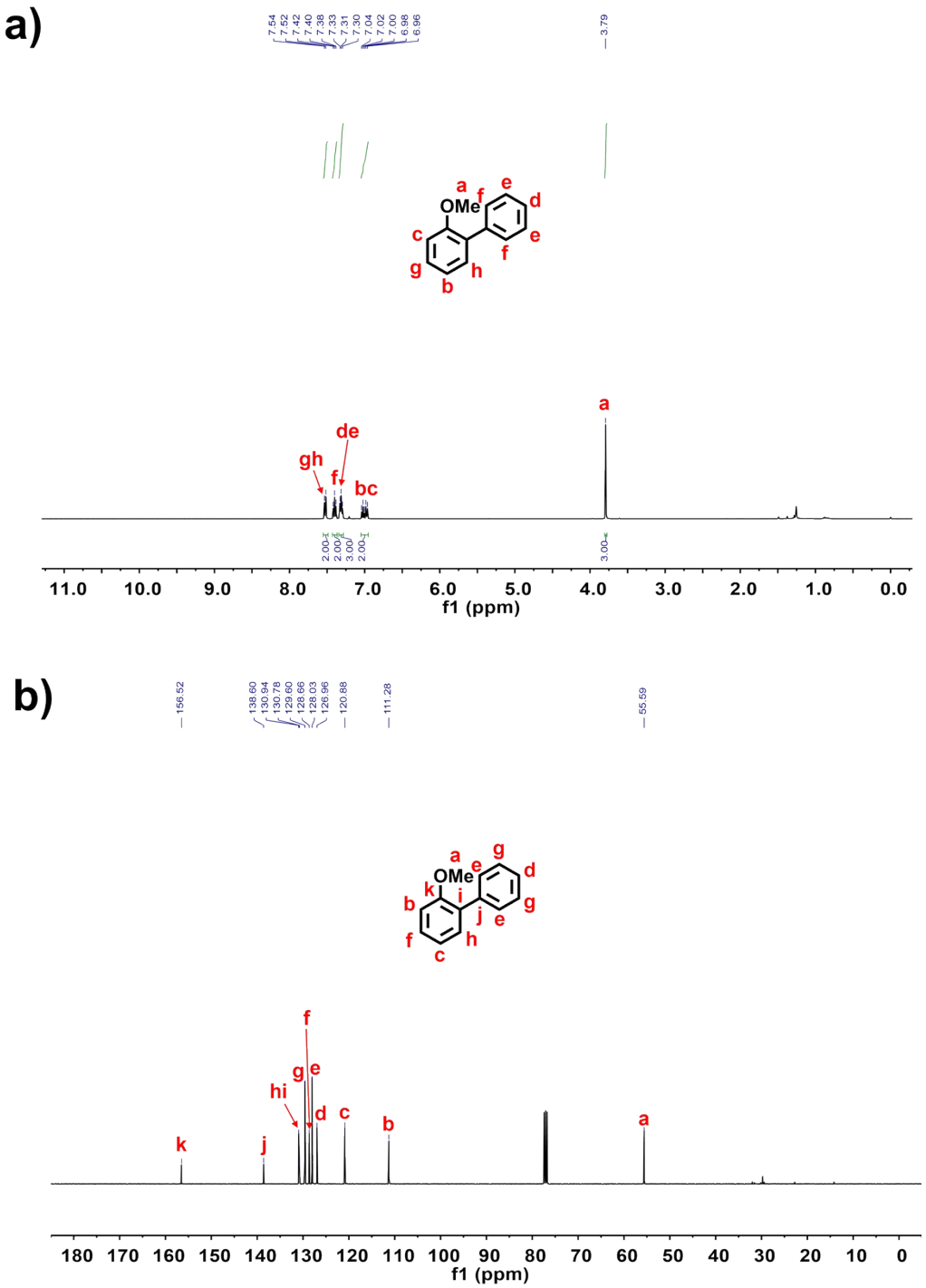

Fig. S24. Characterization of 2-methoxybiphenyl. a) ^{1}H-NMR (400 MHz, $CDCl_3$, ppm): δ=7.52 (d, J=8 Hz, 2H), 7.40 (t, J=8 Hz, 2H), 7.31 (m, 3H), 7.00 (m, 2H), 3.79 (s, 3H). b) ^{13}C-NMR (100 MHz, $CDCl_3$, ppm): δ=156.52, 138.60, 130.94, 130.78, 129.60, 128.66, 128.03, 126.96, 120.88, 111.28, 55.59.

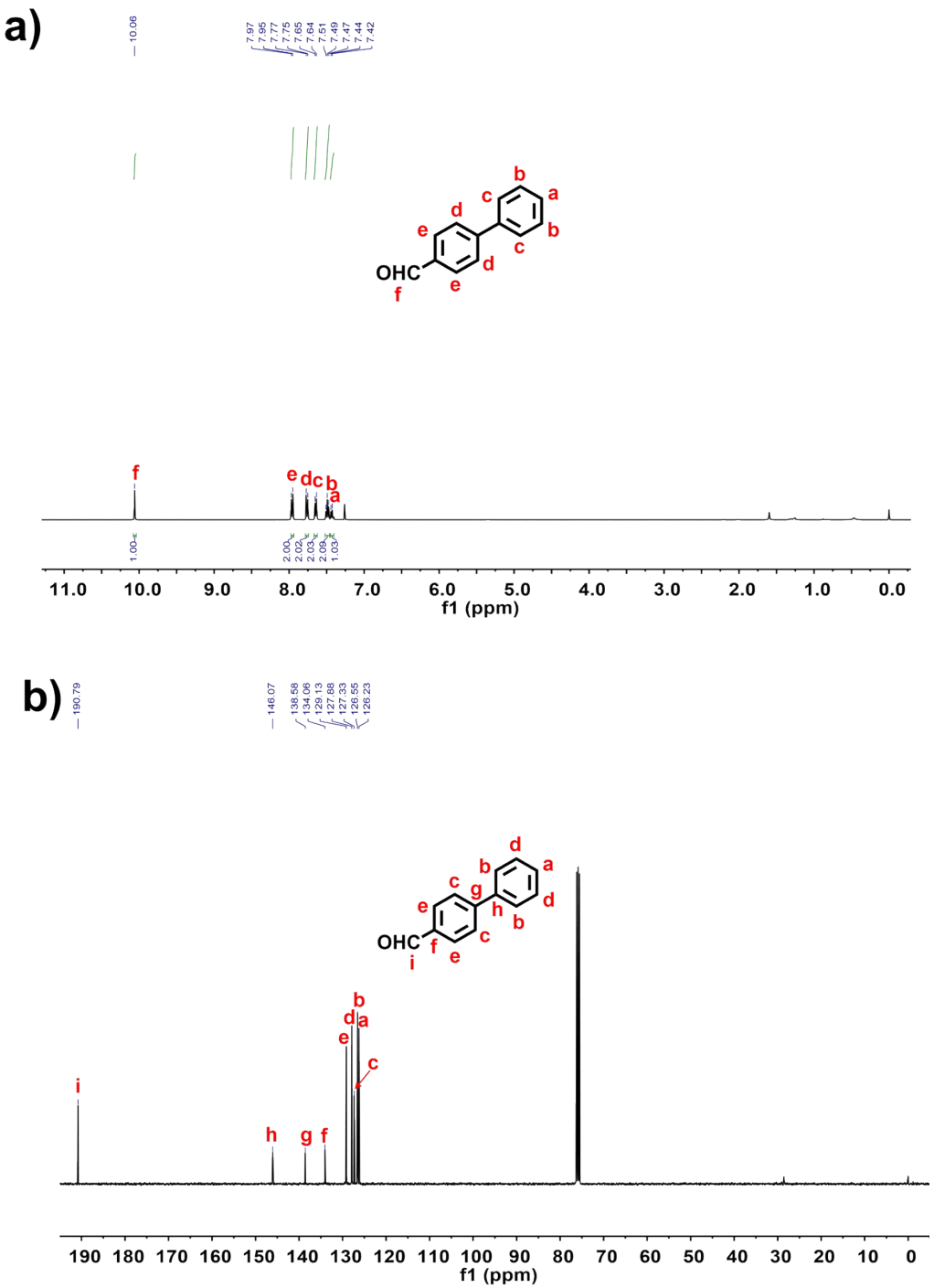

Fig. S25. Characterization of 4-biphenylcarboxaldehyde. a) ^{1}H-NMR (400 MHz, $CDCl_3$, ppm): δ=10.05 (s, 1H), 7.95 (d, *J*=8 Hz, 2H), 7.75 (d, *J*=8 Hz, 2H), 7.64 (d, *J*=8 Hz, 2H), 7.49 (t, *J*=8 Hz, 2H), 7.42 (t, *J*=8 Hz, 1H). b) ^{13}C-NMR (100 MHz, $CDCl_3$, ppm): δ=190.79, 146.07, 138.58, 134.06, 129.13, 127.88, 127.33, 126.55,126.23.

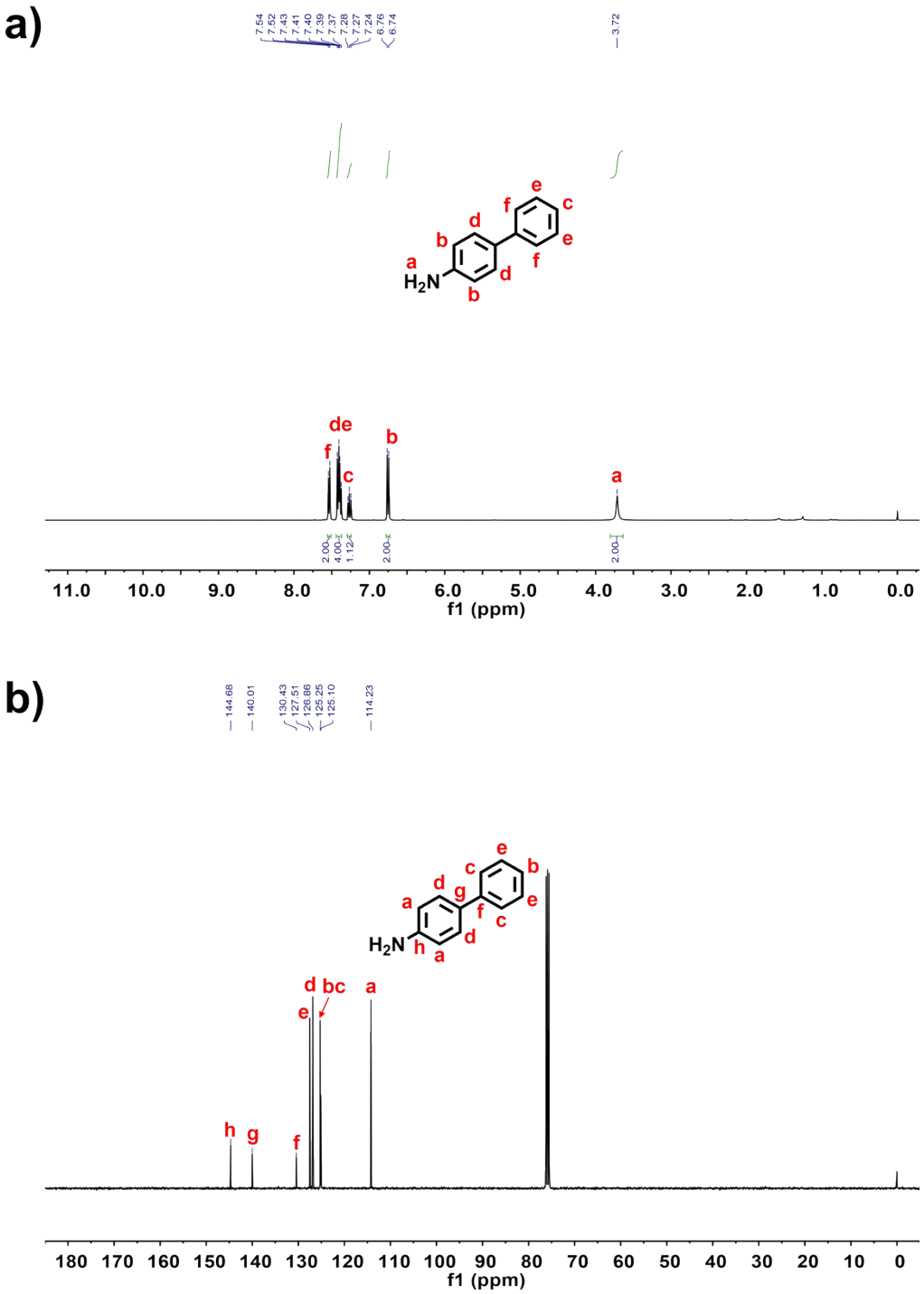

Fig. S26. Characterization of 4-aminobiphenyl. a) ^{1}H-NMR (400 MHz, $CDCl_3$, ppm): δ=7.52 (d, J=8 Hz, 2H), 7.40 (m, 4H), 7.27 (t, J=4 Hz, 1H), 6.74 (d, J=8 Hz, 2H), 3.72 (s, 2H). b) ^{13}C-NMR (100 MHz, $CDCl_3$, ppm): δ=144.68, 140.01, 130.43, 127.51, 126.88, 125.25, 125.10, 114.23.

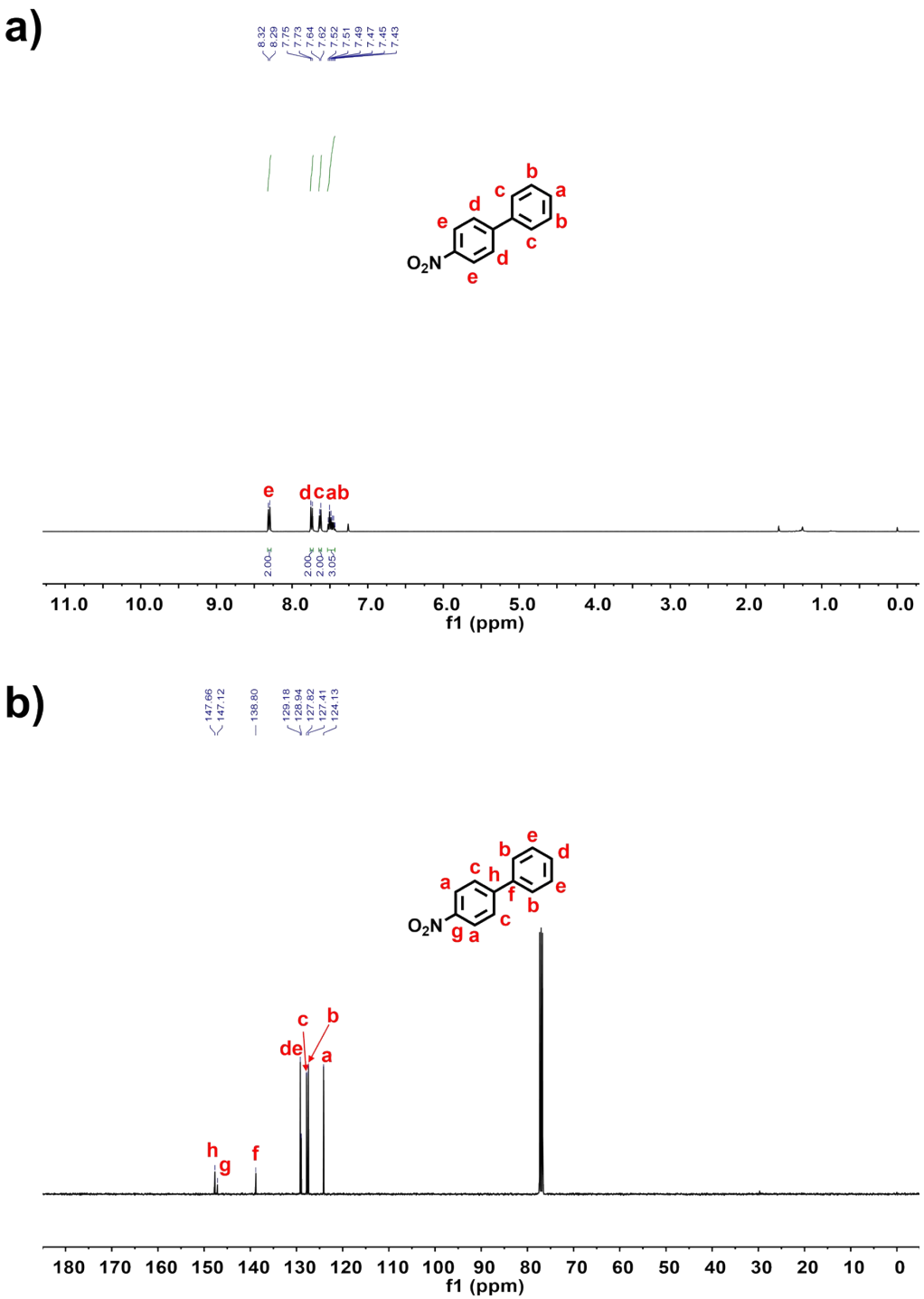

Fig. S27. Characterization of 4-nitrobiphenyl. a) ^{1}H-NMR (400 MHz, $CDCl_3$, ppm): δ=8.29 (d, J=12 Hz, 2H), 7.73 (d, J=8 Hz, 2H), 7.62 (d, J=8 Hz, 2H), 7.49 (m, 3H). b) ^{13}C-NMR (100 MHz, $CDCl_3$, ppm): δ=147.86, 147.12, 138.80, 129.18, 128.94, 127.82, 127.41, 124.13.

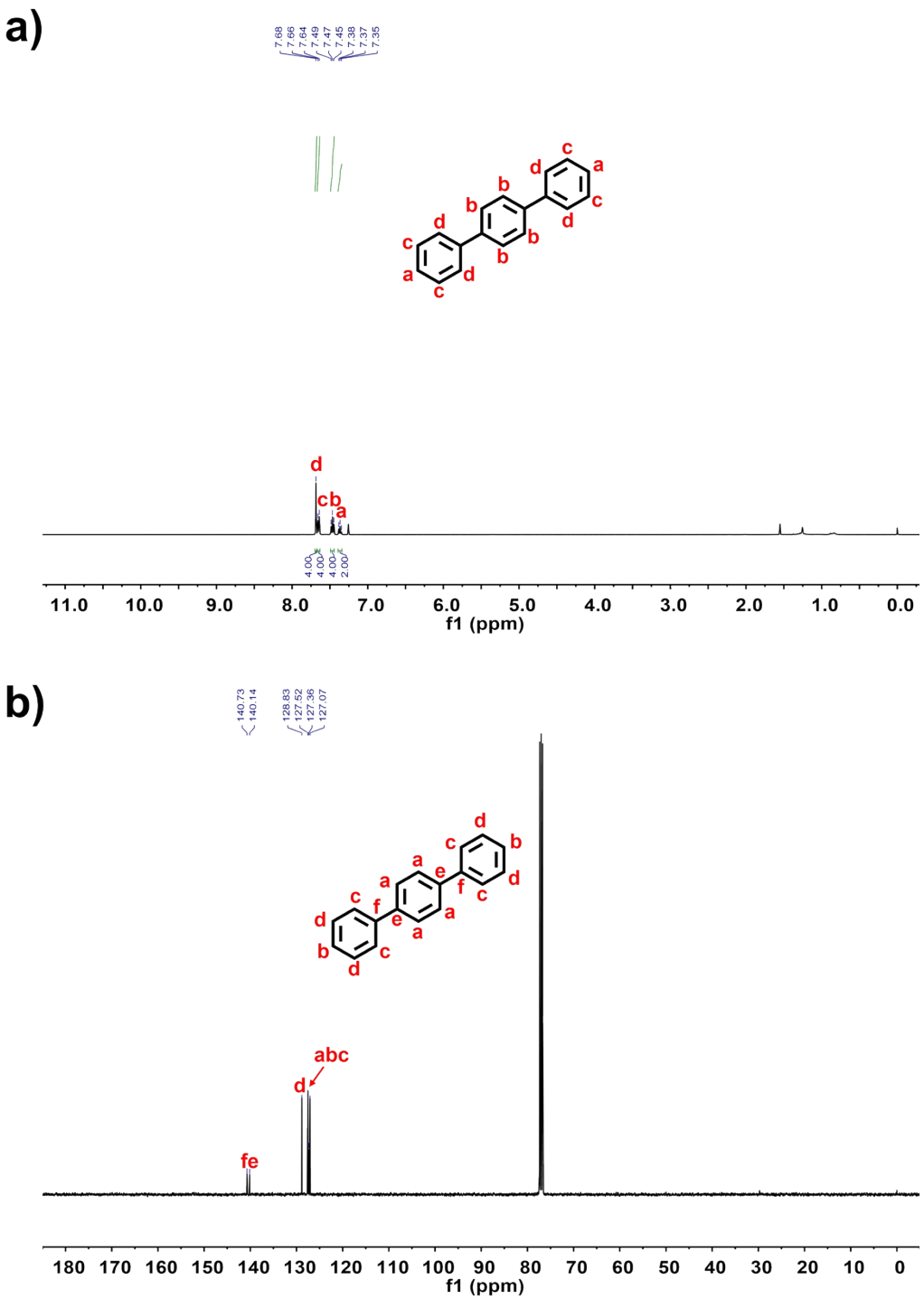

Fig. S28. Characterization of p-terphenyl. a) ^{1}H-NMR (400 MHz, $CDCl_3$, ppm): δ=7.68 (s, 4H), 7.64 (d, J=8 Hz, 4H), 7.47 (t, J=8 Hz, 4H), 7.37 (t, J=8 Hz, 2H). b) ^{13}C-NMR (100 MHz, $CDCl_3$, ppm): δ=140.73, 140.14, 128.83, 127.52, 127.36, 127.07.

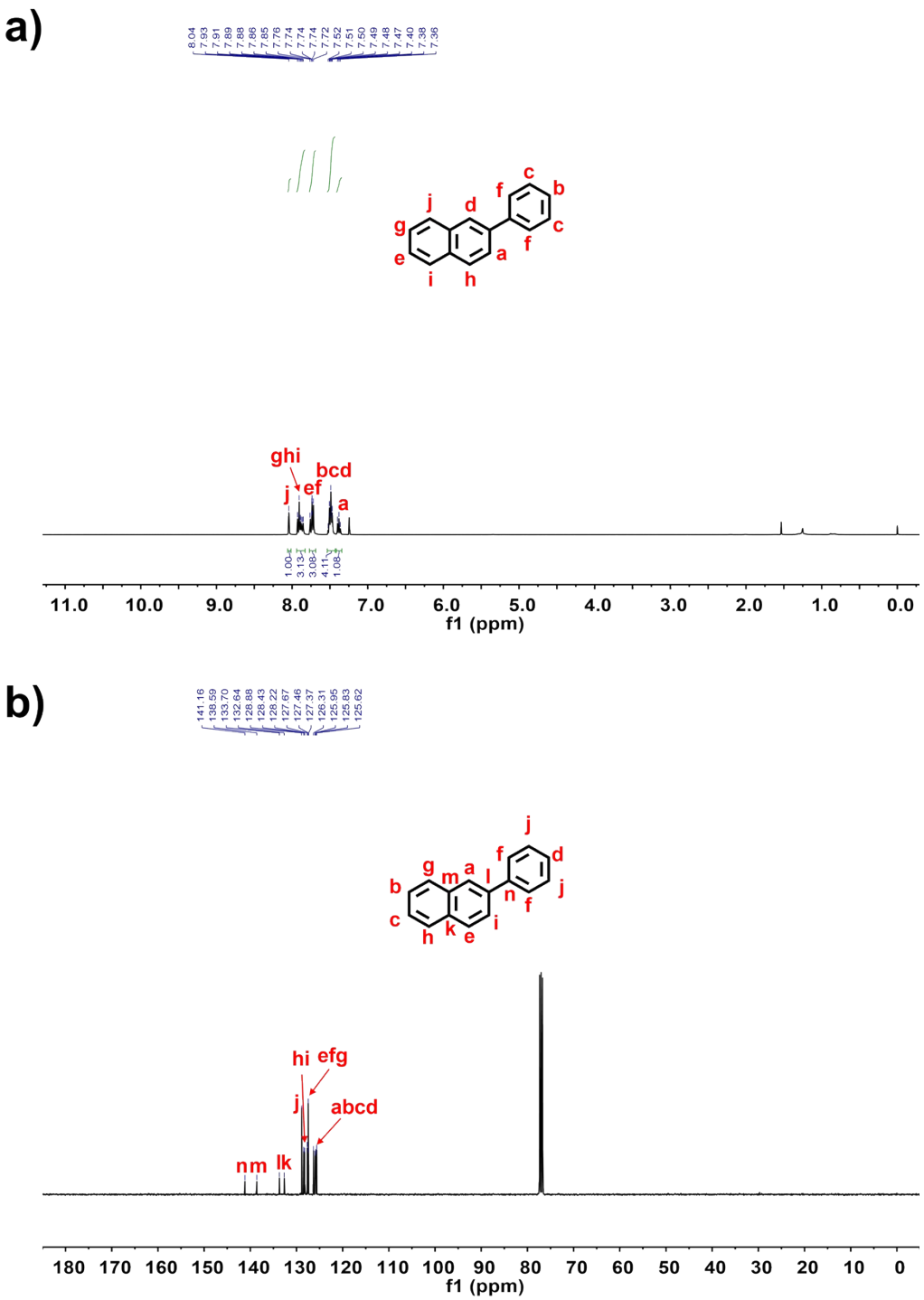

Fig. S29. Characterization of 2-phenylnaphthalene. a) ^{1}H-NMR (400 MHz, $CDCl_3$, ppm): δ=8.04 (s, 1H), 7.89 (m, 3H), 7.74 (m, 3H), 7.49 (m, 4H), 7.38 (m, 1H). b) ^{13}C-NMR (100 MHz, $CDCl_3$, ppm): δ=141.16, 138.59, 133.70, 132.64, 128.88, 128.43, 128.22, 127.67, 127.46, 127.37, 126.31, 125.95, 125.83, 125.62.

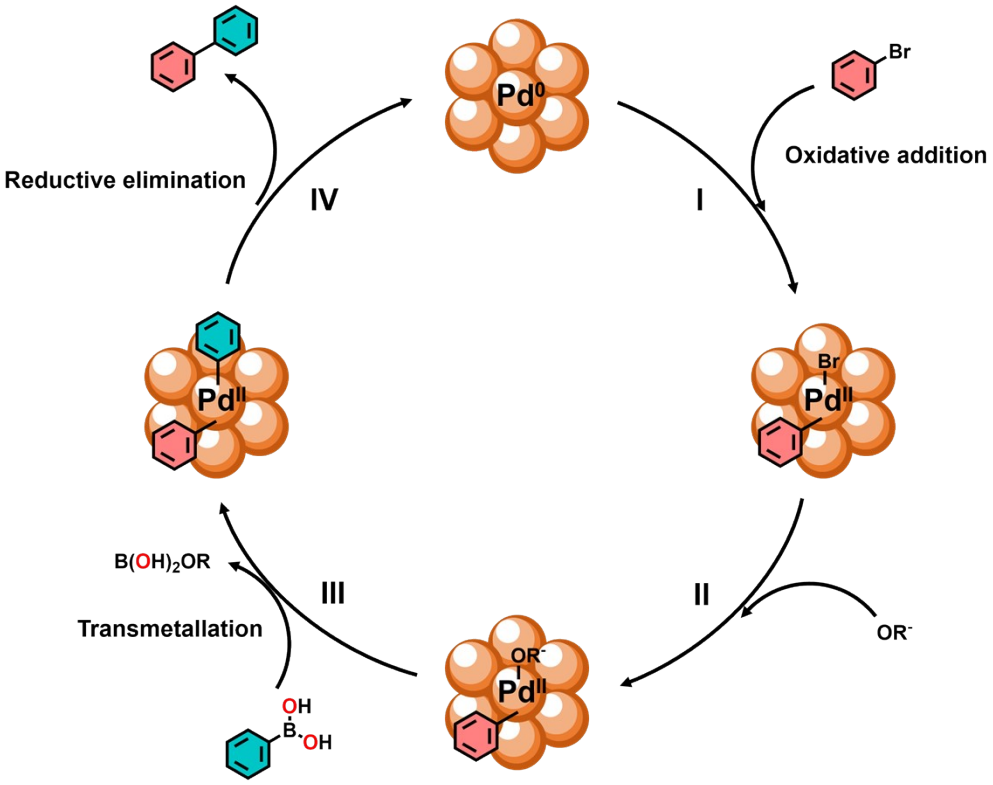

Fig. S30. Proposed catalytic cycle for the Suzuki-Miyaura cross-coupling reaction catalyzed by **Pd@AABH-TFBT-COF**, using bromobenzene and phenylboronic acid as the model substrates. The cycle proceeds through three fundamental steps: (I) Oxidative addition: The Pd(0) active species inserts into the C-Br bond of bromobenzene, forming an aryl-Pd(II)-Br intermediate. (II and III) Transmetalation: In the presence of K_2CO_3, phenylboronic acid is activated to generate a tetracoordinate borate species $[Ph\text{-}B(OH)_2OR]^-$. This species transfers the phenyl group to the palladium center, yielding a diaryl-Pd(II) complex (Ph-Pd(II)-Ph). (IV) Reductive elimination: The diaryl-Pd(II) complex undergoes C-C bond formation to release biphenyl and regenerate the Pd(0) catalyst, which then enters the next catalytic cycle.

7. References

1 D. S. Bohle, Z. Chua, M. Singer Hobbs, I. Perepichka and A. Waked, *Chem. Eur. J.*, 2015, **21**, 13739–13747.

2 H. Jin, C. Zhang, P. Liu, X. Ge and S. Zhou, *Appl. Organomet. Chem.*, 2022, **36**, e6642.

3 J.-C. Wang, C.-X. Liu, X. Kan, X.-W. Wu, J.-L. Kan and Y.-B. Dong, *Green Chem.*, 2020, **22**, 1150–1155.

4 X. Wang, J. Li, L. Wang and M. Szostak, *J. Org. Chem.*, 2025, **90**, 6532–6537.

5 S.-Y. Ding, J. Gao, Q. Wang, Y. Zhang, W.-G. Song, C.-Y. Su and W. Wang, *J. Am. Chem. Soc.*, 2011, **133**, 19816–19822.

6 H. Pan, N. Wang and G.-W. Wang, *Chem. Commun.*, 2025, **61**, 8184–8187.

7 K. Lv, G. Yan, G. Wang, Z. Chen and J. Hu, *Catal. Lett.*, 2023, **153**, 2959–2974.

8 Y. Nailwal, M. A. Addicoat, M. Gaurav and S. K. Pal, *ACS Appl. Nano Mater.*, 2023, **6**, 1714–1723.

9 C. Krishnaraj, H. S. Jena, K. S. Rawat, J. Schmidt, K. Leus, V. Van Speybroeck and P. Van Der Voort, *ACS Appl. Mater. Interfaces*, 2022, **14**, 50923–50931.

10 Y. Liu, C. Wu, Q. Sun, F. Hu, Q. Pan, J. Sun, Y. Jin, Z. Li, W. Zhang and Y. Zhao, *CCS Chem.*, 2020, **3**, 2418–2427.

11 J. Liu, H. Zhan, N. Wang, Y. Song, C. Wang, X. Wang, L. Ma and L. Chen, *ACS Appl. Nano Mater.*, 2021, **4**, 6239–6249.

12 G. Wang, Z. Chen, G. Yan and J. Hu, *New J. Chem.*, 2023, **47**, 297–306.

13 C. Qian, W. Zhou, J. Qiao, D. Wang, X. Li, W. L. Teo, X. Shi, H. Wu, J. Di, H. Wang, G. Liu, L. Gu, J. Liu, L. Feng, Y. Liu, S. Y. Quek, K. P. Loh and Y. Zhao, *J. Am. Chem. Soc.*, 2020, **142**, 18138–18149.

14 G. Wang, Z. Hu, Z. Chen, J. Wang, J. Hu and X. Xu, *Appl. Surf. Sci.*, 2023, **631**, 157538.

15 M. Bashri, S. Kumar, P. Bhandari, S. Stephen, M. J. O'Connor, S. Gaber, T. Škorjanc, M. Finšgar, G. E. Luckachan, B. Belec, E. Alhseinat, P. S. Mukherjee and D. Shetty, *ACS Appl. Mater. Interfaces*, 2025, **17**, 17804–17812.

16 T. Chen, L. Chen, Q. Li, C. Zhou, L. Dong, L. Tan, C. Lu and Z. Liu, *ACS Appl. Mater. Interfaces*, 2025, **17**, 42225–42232.

17 A. Hassan, A. Kumar, S. A. Wahed, S. Mondal, A. Kumar and N. Das, *Nanoscale*, 2025, **17**, 4765–4775.

18 L. Li, Q. Shan, J. Zang, L. Yu, D. J. Young, Z.-G. Ren and H.-X. Li, *Catal. Sci. Technol.*, 2024, **14**, 7212–7218.

19 I. Romero-Muñiz, A. Mavrandonakis, P. Albacete, A. Vega, V. Briois, F. Zamora and A. E. Platero-Prats, *Angew. Chem. Int. Ed.*, 2020, **59**, 13013–13020.

20 F. Shukla, M. Patel, Q. Gulamnabi and S. Thakore, *Dalton Trans.*, 2023, **52**, 2518–2532.

21 N. Brown, Q. Zhang, Z. Alsudairy, C. Dun, Y. Nailwal, A. Campbell, C. Harrod, L. Chen, S. Williams, J. J. Urban, Y. Liu and X. Li, *ACS Sustain. Chem. Eng.*, 2024, **12**, 13535–13543.

22 Y. Hou, X. Zhang, J. Sun, S. Lin, D. Qi, R. Hong, D. Li, X. Xiao and J. Jiang, *Microporous Mesoporous Mater.*, 2015, **214**, 108–114.

23 T. Chen, Y. Pang, S. H. Ali, L. Chen, Y. Li, X. Yan and B. Wang, *Mol. Catal.*, 2024, **558**, 114045.

24 Z. Tao, Q. Zhang, Q. Xie, H. Qu, Y. Liu, L. Kong, G. Xu, S. Zhang and Z. Zhou, *Surf. Interfaces*, 2024, **55**, 105313.